Detailed Study of ^{4}He Nuclei through Response Function Separations at High Momentum Transfers

— Jeopardy Defense of Proposal E04-107 —

K. Aniol (spokesperson), M. Epstein, and D. Margaziotis

California State University, Los Angeles, CA 90032, USA

F. Benmokhtar (spokesperson)

University of Maryland, College Park, MD 20742, USA
Carnegie Mellon University, Pittsburgh, PA 15213, USA (starting 01/2008)

W. Bertozzi, S. Gilad (spokesperson), J. Huang, B. Moffit, P. Monaghan, N. Muangma, A. Puckett, N. Sparveris, and X. Zhan

Massachusetts Institute of Technology, Cambridge, MA 02139, USA

J.P. Chen, E. Chudakov, J. Gomez, J.-O. Hansen, D.W. Higinbotham (spokesperson), C.W. de Jager, J.-M. Laget, J. LeRose, A. Saha (spokesperson) [1], and B. Wojtsekhowski

Jefferson Lab, Newport News, VA 23606, USA

J.M. Udias, J.L. Herraiz, M.C. Martinez,

Universidad Complutense de Madrid, Spain

M. Mihovilovič, M. Potokar, and S. Širca

Department of Physics, University of Ljubljana, Slovenia

C.F. Perdrisat

College of William and Mary, Williamsburg VA 23187, USA

P. Markowitz

Florida International University, Miami, FL 33199, USA

E. Cisbani, F. Cusanno, F. Garibaldi, S. Frullani, M. Iodice, and G.M. Urciuoli

INFN, Laboratorio di Fisica, I-00161 Rome, Italy

J. R. Vignote,
Gesellschaft fr Schwerionenforschung mbH, D-64291 Darmstadt, Germany

L. Weinstein
Old Dominion University, Norfolk, VA 23529, USA

E. Piasetzky, G. Ron, I. Pomerantz, and R. Shneor
Tel Aviv University, Tel Aviv, Israel

B. Sawatzky and Z.-E. Meziani
Temple University, Philadelphia, PA 19122, USA

K.G. Fissum
University of Lund, Box 118, SE-221 00 Lund, Sweden

J. Calarco
University of New Hampshire, NH 03824, USA

D. Day, R. Lindgren, B.E. Norum, R. Subedi, and K. Wang,
University of Virginia, Charlottesville, VA 22901, USA

C. Ciofi degli Atti and M. Alvioli
University of Perugia, I-06100 Perugia, Italy

H. Morita
Sapporo Gakuin University, Japan

A.F. Amroun
Université des Sciences et de la Technologie. USTHB d'Alger, Algérie

L. Kaptari
Laboratory of Theoretical Physics, Dubna, Russia

Sabine Jeschonnek
Ohio State University, Columbus, Ohio

and

The Hall A Collaboration

Abstract

We propose a detailed study of ^{4}He structure and reaction dynamics through ^{4}He(e,e′p) coincidence measurements at high momentum transfers. In perpendicular kinematics, this will be accomplished by measuring the quasi-elastic ^{4}He(e,e′p)^{3}H cross section at a fixed $\mathbf{q} = 1.50$ GeV/c and $\omega = 0.84$ GeV as a function of missing momentum up to 1.2 GeV/c. We shall also extract the response function R_{TL} and the left-right asymmetry A_{TL} up to $p_m = 0.5$ GeV/c, and extract R_T and R_{L+TT} for missing momenta around 0 GeV/c, 0.4 GeV/c, and 0.5 GeV/c. In parallel kinematics, we shall study the Q^2 dependence of the reaction ^{4}He(e,e′ p)^{3}H by performing a longitudinal/transverse R_L/R_T separation from protons emitted along $\mathbf{q}$ in the Q^2 range from 0.81 to 4.1 [GeV/c]^2 with missing momenta near zero. To investigate nucleon-nucleon correlations, we shall also make R_L/R_T separations of the reaction ^{4}He(e,e′ p)pnn at $x_B = 1.86$ for high missing momentum, $p_m = 0.4$ GeV/c, and for a $\mathbf{q}$ of 1.5 GeV/c. An additional measurement, which has been added since the last review, is a short addition to the recently approved ^{4}He(e,e′pN) SRC experiment where we propose to measure the entire range of missing momentum from p_m= 0.0-0.9 GeV/c of the ^{4}He(e,e′p) reaction at a Q^2= 2 [GeV/c]^2 and $x_B = 1.2$ instead of just the p_m = 0.4-0.9 GeV/c that was requested by the Hall A SRC group. Taken together, these measurements will provide detailed observables to test current and future theoretical models with a nucleus where one can do both exact calculations and mean field calculations. The measurements will be performed in Hall A using the two high resolution spectrometers and a cryogenic ^{4}He target (i.e. only standard equipment is needed for these measurements).

[1] contact person: A. Saha, phone: (757) 269-7605, e-mail: saha@jlab.org

Contents

1 Preface

^{4}He is an essential element in developing "conventional nuclear physics" calculations. It is the simplest nuclear system in which all the basic ingredients of a complex nuclei exist. Its binding energy is similar to that of heavier nuclei and it is reasonable to expect that the behavior of nucleon pairs within this nucleus is similar to that inside heavier nuclei. It is a tightly bound system with strong correlations, providing a better environment for the study of short range effects and nucleon-nucleon correlations in nuclei. Moreover, its study provides an important connection between two- and three-body systems, where exact calculations are possible in both initial and final states of the (e,e′p) reaction, and heavier nuclei where microscopic many body calculations still remain intractable.

We propose a detailed study of the electromagnetic structure of ^{4}He through (e,e′p) coincidence measurements at high momentum transfers. In perpendicular kinematics, this will be accomplished by measuring the quasi-elastic ^{4}He(e,e′p)^{3}H cross section at a fixed $\mathbf{q} = 1.50$ GeV/c and $\omega = 0.84$ GeV as a function of missing momentum up to 1.2 GeV/c. We shall also extract the response function R_{TL} and the left-right asymmetry A_{TL} up to $p_m = 0.5$ GeV/c, and extract R_T and R_{L+TT} for missing momenta around 0 GeV/c, 0.4 GeV/c, and 0.5 GeV/c. These measurements will provide detailed observables to test current and future theoretical models. In parallel kinematics, we shall study the Q^2 dependence of the reaction ^{4}He(e,e′p)^{3}H by performing a longitudinal/transverse R_L/R_T separation from protons emitted along $\mathbf{q}$ in the Q^2 range from 0.81 to 4.1 [GeV/c]^2 with missing momenta near zero. We shall also make R_L/R_T separations of the reaction ^{4}He(e,e′p)pnn for high missing momentum, $p_m = 0.4$ GeV/c, for a $\mathbf{q}$ of 1.5 GeV/c and $x_B = 1.86$ to investigate nucleon-nucleon correlations. These measurements will be performed in Hall A, using the two high resolution spectrometers and a cryogenic ^{4}He target. Hall A is the only facility in the world where such measurements can be performed.

In addition to the range of kinematics of the previous proposal, we are asking for 0.5 PAC days to extend the ^{4}He(e,e′p) measurements that will be done during the E07-006 experiment to low Q^2. The approved triple coincidence experiment E07-006 only proposed to measure in the region where correlations are expected to dominate. We propose here to map out the entire region from p_m of 0 to 845 MeV for the (e,e′p) reaction to extend our understanding of the momentum distribution of nucleons in the nucleus (i.e. the original motivation for the early (e,e′ p) experiments). This is a unique opportunity to do measurements at large Q^2 and large-x where the competing mechanisms are expected to be small. It is worth noting that early Jefferson Lab proposals stated that large Q^2 at x=1 would be sufficient to do this; but experiments have shown this not to be the case.

With this extension, we shall cover with the constant (q, ω) kinematics the (e,e′p) reaction over the small Pmiss region: E = 4.627 GeV and $Q^2 = 2$ [GeV/c]^2 for $p_m = 100$, 200 and 300 MeV/c along with the 400 - 845 MeV/c that will be taken as a by-product of the (e,e′ pN) experiment.

2 Progress Since PAC 26

When this proposal was approved the first time by PAC 20, our sister ^{3}He experiment, E89-044, had successfully completed taking data. The E89-044 experiment was done on the ^{3}He(e,e′p)X reaction in nearly identical kinematics as proposed herein for ^{4}He. As is explained in this proposal, one of the overarching goals of our collaboration of experimentalists and theorists is to obtain high precision data on both ^{3}He and ^{4}He (one loosely bound few-body system and one tightly bound, closed-shell few-body system) with very well defined kinematics; which, when combined with the Hall A ^{16}0(e,e′p) results, could bridge the gap between microscopic calculations which use an exact wave-function and the calculations for heavy nuclei which successfully reproduce the experimental results with mean-field calculations.

The E89-044 experimental results have been published in PRL [1,2] and the long paper is in the writing phase. The results have generated much theoretical interest as evidenced by the calculations from Jean-Marc Laget, Jose Udias, and Ciofi degli Atti. A sample of the E89-044 experimental results and theoretical calculations can be seen in Section 6.1. Combining the E89-044 data with the data proposed herein would provide theorists with results from observables such as A_{TL}, which is extremely sensitive to the reaction dynamics, for ^{3}He and ^{4}He for the same kinematics. Since microscopic calculations can be done for both nuclei, these type of data can refine our understanding of few-body systems and, for example, allow a separation of density dependent effects from other dynamics. Also, as the lab starts to prepare for the 12 GeV upgrade, it is clear that thoroughly understood, high quality base-line data are necessary to facilitate the future separation of QCD effects in (e,e′p), such as color transparency, from nucleon-meson effects.

Other experimental results which have become available since PAC 20 are the measurements from the E97-111 experiment on ^{4}He(e,e′p)^{3}H at high missing momentum. This experiment measured cross sections of the ^{4}He(e,e′p)^{3}H reaction in the region where plane-wave calculations predict a minimum in the cross section. The preliminary results, shown in section 6.2, show no dip. New calculations from theorist such as Jean-Marc Laget, Jan Ryckebusch, Hiko Morita and Ciofi degli Atti indicate this is most likely due to reaction dynamics causing the dip region to be filled. For the experiment proposed here, we will be able to extract for the first time the R_{LT}, $R_L + R_{TT}$, and R_T response functions in this interesting kinematical region. While there is no clear dip in any of the modern cross section calculations for these kinematics, the different models predict different magnitudes and slopes of the response functions.

Our sister experiment, E89-044, educated three Ph.D. students: Marat Rvachev (MIT) on the perpendicular kinematics two-body break-up channels, Emilie Penel (Grenoble) on the parallel kinematic two-body break-channels, and Fatiha Benmokhtar (Rutgers) on the three-body break-up channels. All the three theses are completed [3–5]. We expect this experiment would educate a similar number of students.

3 Overview of Goals

We propose to study the structure and electromagnetic currents in ^{4}He using the ^{4}He(e,e′p) reaction. We intend to concentrate on aspects which can be uniquely measured in Hall A. In particular, we intend to measure the ^{4}He(e,e′p)^{3}H cross section in constant electron kinematics up to missing momentum of about 1.2 GeV/c, and to separate response functions in regions where their selective sensitivity to the various nuclear currents can provide an important means for understanding the measured observables. Due to the large momentum acceptance of the spectrometers, we will simultaneously obtain data in the missing-energy continuum.

The proposed measurements can be divided into "perpendicular" (non-parallel) and parallel kinematics (see Section 4 for details). The perpendicular kinematics are suitable for measuring the cross sections in constant transferred momentum and energy up to very high missing energy. They are also needed for the separation of the longitudinal-transverse interference response, R_{TL}, and the left-right asymmetry A_{TL}. By going to different virtual photon polariztions ϵ, we will be able to separate the transverse response, R_T, and a combination of the longitudinal and transverse-transverse interference responses, denoted in this proposal as R_{L+TT}. All observables can be measured with the same transferred momentum and energy, hence fixed kinematic conditions. In parallel kinematics, a unique separation of R_L and R_T can be obtained. However, because of the constraint imposed by fixing the angle between the transfered momentum and the ejected proton, varying the missing momentum requires varying either the transferred momentum or energy, resulting in significant changes in kinematic conditions.

We shall use perpendicular kinematics to measure the ^{4}He(e,e′p)^{3}H cross section in quasi-elastic kinematics for missing momentum, p_m, in the range 0 GeV/c to 1.20 GeV/c by varying the angle between the transferred momentum $\mathbf{q}$ and the ejected protons. This will be done at fixed electron kinematics: a fixed beam energy of 4.80 GeV, a fixed three-momentum transfer $\mathbf{q}$ of 1.50 GeV/c, and fixed energy transfer of 0.840 GeV. This will extend substantially the set of available data which currently extend only to p_m = 0.690 GeV/c [6,7] but were obtained in various electron kinematics due to the limitations of the facility. Our measurements will be performed in one quasi-elastic kinematics. In addition, it is predicted that our proposed measurements at much higher transferred momentum and energy (and hence high ejected-proton energies) provide better handles on effects such as final-state interactions (FSI) and suppress meson-exchange currents (MEC) and isobar currents (IC).

For the missing momentum range 0 GeV/c to 0.500 GeV/c, we shall measure also the R_{TL} response and the A_{TL} asymmetry. This is done by measuring the cross sections for ejected protons on both sides of the transferred momentum vector. R_{TL} and A_{TL} have been shown to be sensitive to broken factorization which in the case of ^{4}He is predicted to result from relativistic dynamical effects and interference between the plane-wave and re-scattering amplitudes [8]. These observables will provide important additional constraints to modern

model calculations currently being developed within both microscopic framework and relativistic distorted wave impulse approximation (RDWIA).

Finally, for missing momentum of around 0 GeV/c, 0.400 GeV/c, and 0.500 GeV/c, we shall perform additional measurements at the same transferred momentum and energy, but at different electron beam energies (and hence electron angle and virtual-photon polarization). This will enable the separation of R_T and R_{L+TT} responses in bins of 25 MeV/c between 0.325 and 0.575 GeV/c. All PWIA models predict a dip in the cross section in this p_m range due to suppression of the s-state ground-state wave function. This dip was not observed in measurements at NIKHEF [7] nor in recent Jefferson Lab measurements [9]. By measuring for the first time the response functions in this p_m, we shall gain further understanding of this interesting kinematical region by testing whether theory can correctly reproduce both cross section and the response functions.

In parallel kinematics we shall perform a Rosenbluth separation of the R_L and R_T responses for low missing momenta as a function of three transfer momenta for $\mathbf{q}$ = 1.0 — 3.0 GeV/c. All measurements will be done in quasi-elastic kinematics. Previous Saclay data [10] taken at $\mathbf{q}$ = 0.3 GeV/c to 0.7 GeV/c note a sizeable quenching of the longitudinal response at p_m = 0.09 GeV/c. Inclusive ^{4}He(e,e') data note a quenching of the longitudinal response as well. No such quenching was observed for ^{3}He in either inclusive scattering [11] or exclusive scattering [12] measurements. For low missing momenta, the R_L and R_T responses should behave more like those of the proton as the transfered momentum is increased. We hope to observe the transition from a quenched longitudinal response to the predicted value with increased transferred momentum. Similar measurements were performed in Hall A on ^{3}He in same kinematic conditions, so the proposed measurement on ^{4}He will also provide information about nuclear density effects.

Finally, we would like to separate the R_L and R_T responses at p_m = 0.400 GeV/c at $\mathbf{q}$ = 1.5 GeV/c in anti-parallel kinematics. In this kinematic setting we will make use of the large energy acceptance of the spectrometers to measure both the two-body breakup and continuum. In anti-parallel measurements (x_B = 1.86), two-body currents as well as final state interactions are expected to be suppressed while short-range correlations are predicted to be observed [13]. Short-range correlations are predicted to be predominantly longitudinal while two-body processes are expected to be transverse in nature.

4 Kinematics

The kinematics for the (e,e′p) reaction are shown in Fig. 1. The scattering plane is defined by the incoming electron, $e = (E_e, \mathbf{e})$, and the outgoing electron, $e' = (E'_e, \mathbf{e}')$. The four-momentum of the virtual photon is given by q=(w, $\mathbf{q}$) and the four-momentum of the outgoing proton is given by $p' = (E_p, \mathbf{p}')$. The four-momentum square, $Q^2 = q^2 - \omega^2$, is defined such that for electron scattering Q^2 is always positive. The missing momentum vector is defined as $\mathbf{p}_m = \mathbf{q} - \mathbf{p}'$.

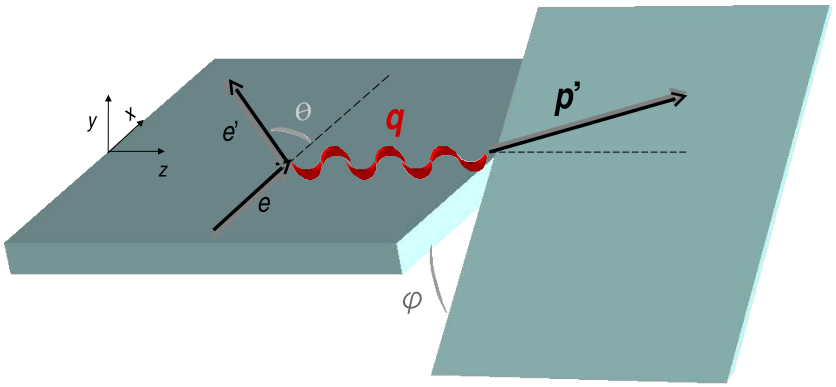

Fig. 1. A schematic of the kinematics for the (e,e′p) reaction.

The form of the differential cross section for the (e,e′p) reactions in the one-photon exchange approximation for without polarization is:

$$\frac{d^6\sigma}{d\Omega_{e'} dE_{e'} d\Omega_{p'} dE_{p'}} = \frac{E_p p_p}{(2\pi)^3} \sigma_{Mott} \left[v_T R_T + v_L R_L + v_{TL} R_{TL} \cos\phi + v_{TT} R_{TT} \cos 2\phi \right], \quad (1)$$

$$(2)$$

with ϕ the angle between the plane defined by $\mathbf{e}$ and $\mathbf{e}'$ and the plane defined by $\mathbf{p}'$ and $\mathbf{q}$, σ_M is the Mott cross section,

$$\sigma_{Mott} = \frac{4\alpha^2 E_{e'}^2}{Q^4} \cos^2 \frac{\theta_{e'}}{2}. \quad (3)$$

The kinematics factors v_L, v_T, v_{TL},and v_{TT} are:

$$v_L = \frac{Q^4}{\mathbf{q}^4}, \quad (4)$$

$$v_T = \frac{Q^2}{2\mathbf{q}^2} + \tan^2(\theta_e/2), \tag{5}$$

$$v_{TL} = \frac{Q^2}{\mathbf{q}^2}\left[\frac{Q^2}{\mathbf{q}^2} + \tan^2(\theta_e/2)\right]^{1/2}, and \tag{6}$$

$$v_{TT} = \frac{Q^2}{2\mathbf{q}^2}. \tag{7}$$

$$\tag{8}$$

For the two body break-up channel, ^{4}He(e,e′p)^{3}H, the proton energy and angle with respect to $\mathbf{q}$ are correlated because the missing energy is fixed. In this case the differential cross section is written as follows:

$$\frac{d^5\sigma}{d\Omega_{e'}d\Omega_{p'}dE_{e'}} = \frac{E_p P_p}{(2\pi)^3}\sigma_{Mott} f_{rec}^{-1}\left[v_T R_T + v_L R_L + v_{TL} R_{TL}\cos\phi + v_{TT} R_{TT}\cos 2\phi\right], \tag{9}$$

where f_{rec} is the recoil factor,

$$f_{rec} = \left[1 - \frac{E_{p'}}{E_t}\frac{\mathbf{p_m}\cdot\mathbf{p'}}{p'^2}\right]. \tag{10}$$

The response functions, R_L, R_T, R_{TL}, R_{TT} can be separated by a suitable choice of the kinematic parameters. In perpendicular in-plane kinematics, i.e. constant $\mathbf{q}$ and ω kinematics, one can separate R_T, R_{TL}, and a combination of the R_L and R_{TT} response functions, denoted in this proposal as R_{L+TT}. One can also measure the cross section asymmetry A_{TL} for a given $\mathbf{q}$ and ω. This asymmetry is defined as:

$$A_{TL} = \frac{\sigma(\phi = 0) - \sigma(\phi = 180)}{\sigma(\phi = 0) + \sigma(\phi = 180)}. \tag{11}$$

In parallel and anti-parallel kinematics, i.e. when the out-going proton is in the direction of $\mathbf{q}$, one can separate the R_L and R_T response functions. In parallel kinematics p_m points in the opposite direction as $\mathbf{q}$ with $x_B < 1$ while in anti-parallel kinematics p_m points in the same direction as $\mathbf{q}$ with $x_B > 1$ where

$$x_B = \frac{Q^2}{2\ M\omega}, \tag{12}$$

is the Bjorken scaling variable. For $x_B > 1$, the region in ω between the quasi-elastic peak and the elastic peak is being probed; while for $x_B < 1$, the region ω towards the delta peak is being probed. The region in ω between the quasi-elastic peak and delta peak is often referred to as the dip region.

5 Physics Motivation

At present, there is a lot of activity in the field of electron scattering from nuclei at a few GeV aimed at understanding the short range structure of nuclei. It would be ideal to perform theoretical calculations of these processes in a completely microscopic fashion, starting from a Lagrangian. Such an approach would contain explicit relativistic treatments of the nuclear dynamics and the electromagnetic current, as well as a consistent treatment of the initial nuclear state and the in general quite complicated hadronic final state. In practice, for high-energy inelastic electron scattering, it is very difficult to calculate both the nuclear ground state and the final hadronic scattering state consistently in a fully microscopic, relativistic manner. Currently, there are several approximate calculations for particular electro-nuclear reactions available for few-body systems, such as [14,15]. However, it is difficult to extend these approaches for the few-body systems to energies above the pion emission threshold. Considerable effort is being put into this field. Non-relativistic microscopic calculations are available for reactions with ^{3}He and ^{4}He in the framework of Faddeev [16] and variational techniques [17,18]. For ^{4}He, relativistic mean-field calculations are also being employed [19]. Calculations of reactions on few-body systems using Lorentz-integral transform method have been developed [20] and compared to data with success. For heavier nuclei, there are only mean-field calculations available, both non-relativistic and increasingly relativistic as well [19]. These RDWIA calculations have been very successful in describing many cross-section and polarization observables for a wide range of nuclei and transferred momenta.

5.1 Importance of ^{4}He

^{4}He is an essential element in developing "conventional nuclear physics" calculations. It is the simplest nuclear system in which all the basic ingredients of a complex nuclei exist. Its binding energy is similar to that of heavier nuclei and it is reasonable to expect that the behavior of nucleon pairs within this nucleus is similar to that inside heavier nuclei. It is a tightly bound system with strong correlations, providing a better environment for the study of short range effects and nucleon-nucleon correlations in nuclei. Moreover, its study provides an important connection between $A \leq 4$ systems, where exact calculations are possible in both initial and final states of the (e,e$'$p) reaction, and heavier nuclei where microscopic many body calculations still remain intractable.

^{4}He is small enough for the use of variational Monte Carlo techniques, yet large and dense enough to be treated in the framework of mean field. Each approach has different advantages, with one providing a more microscopic insight, and the other in the use of phenomenology and relativity. Indeed, both approaches have been employed successfully to describe electromagnetic reactions at transferred momenta up to a few hundred MeV/c, where a large data set is available. A similarly large data set for ^{4}He is needed in the few GeV/c regime to facilitate the development of theoretical tools to describe the struc-

ture and dynamics which can now be probed. In this respect, studies of both ^{3}He and ^{4}He are needed to evaluate the effects of the transition from 3 to 4 nucleons, and from a less to a much more dense nucleus. Indeed, existing data indicate a significant difference between the two isotopes. For example, in inclusive (e,e′) quasi-elastic scattering, the longitudinal and transverse spectral functions in ^{3}He were observed to be the same, whereas in ^{4}He the transverse spectral function was larger by 30-40%. In exclusive ^{4}He(e,e′p)^{3}H measurements at Saclay a quenching of the longitudinal response by about 35-40% was observed while no such quenching of the longitudinal response was observed for ^{3}He(e,e′p)^{2}H. The proposed measurement on ^{4}He will provide data in similar kinematics to data recently obtained in Hall A on ^{3}He.

5.2 Response Function Separations

Since describing nuclear reactions in general and electrodisintegration in particular requires understanding of the initial bound state, the currents involved, and the hadronic final state, it is not sufficient to measure only cross sections. Theoretical models have various "knobs" to play with, so a good description of the experimental data can be obtained by introducing various ingredients, with no good way to distinguish between success due to these ingredients.

Better understanding of the importance of the various ingredients which go into the theoretical models can be obtained by measuring as many independent observables as possible. A unique tool in this respect is the separation of response functions and asymmetries each of which, in general, is sensitive to a different ingredient in the calculations. We illustrate this point by two recent examples. In the data of J. Gao *et al.* [8] the importance of dynamical relativistic effects was clearly demonstrated by a unique structure in the A_{TL} asymmetry which is predicted by calculations only if these effects are properly included. In the Bates data on the electrodisintegration of the deuteron, their comparison to calculations by Arenhovel and Tjon [21] demonstrates that by measuring R_{TL}, R_{TT} and $R_{TL'}$, it is possible to understand the data in terms of consistent inclusion of FSI, MEC, IC, and relativistic effects [21].

5.3 Overview of Existing Data

The following review of existing data is by no means exhaustive. However, it describes all data which are relevant to this proposal.

Before Jefferson Lab, the most extensive ^{4}He(e,e′p)^{3}H cross section measurement was performed at NIKHEF by van Leeuwe *et al.* [6,7]. The cross section was measured in the dip region with $x_B = 0.29$ at $Q^2 = 0.0115$ GeV/c and with a virtual-photon polarization of 0.63. Using perpendicular kinematics, the cross section was measured for missing momentum in the range of 220-690 MeV/c, as seen in Fig. 2. The measured cross sections for

$p_m < 300$ MeV/c agree well with PWIA calculations by Laget [22], Schiavilla [18] and Nagorny [23,24], While for $p_m > 600$ MeV/c, the measured cross sections agree with these authors' calculations which include different prescriptions for treating FSI, MEC or tree-type and one-loop diagrams. Only Nagorny's calculations describe the data reasonably well for $400 < p_m < 500$ MeV/c.

Jefferson Lab experiment E97-111 [9] completed measurements of the ^{4}He(e,e′p)^{3}H cross section for missing momenta up to 500 MeV/c in both perpendicular and parallel kinematics. Motivated by the NIKHEF experiment, this experiment searched for the predicted minimum around $p_m = 425$ MeV/c with the assumption that parallel kinematics measurements are less sensitive to the final-state interactions, which were presumed to fill the minimum in the NIKHEF experiment. The data are still under analysis; however, preliminary results indicate that the predicted minimum is not observed, see Fig. 11. Additionally, theory, which has been significantly improved in the few years since the experiment was approved, no longer predict a minimum.

Response functions were extracted for the ^{4}He(e,e′p)^{3}H reaction in several experiments. The interference R_{TL} response was measured at Bates [25] in dip kinematics with ($x_B = 0.24$) at $Q^2 = 0.09$ GeV/c. The data were best described by calculations of Schiavilla [18] which include a correlated wave function for the proton-triton scattering state. MEC are required for better agreement with the data. The longitudinal and transverse responses were extracted by Rosenbluth separation in quasi-elastic kinematics at Saclay [10]. The measurements were done at $p_m = 30$, 90, and 190 MeV/c for a range of transfered momenta $\mathbf{q} = 0.3$ - 0.83 (GeV/c)^2. All measurements were done in parallel kinematics. Comparison of the data to the calculations of Schiavilla [17] and Laget [26] resulted in the conclusion that the longitudinal response is quenched by up to 35-40% up to the highest p_m and $\mathbf{q}$. The authors further claim that this quenching may be an indication of the modification of the nucleon form factors in the nuclear medium. No such quenching was observed for the transverse response, nor for either the longitudinal or transverse responses in ^{4}He(e,e′p)^{3}H and ^{2}H(e,e′p)n [10].

Measurements at Mainz were performed with a fixed transfered momentum $\mathbf{q} = 686$ MeV/c. The measurements by R. Florizone *et al.* [27] were performed in quasi-elastic kinematics ($\omega = 243$ MeV) while the measurements by A. Kozlov *et al.* [28,29] were performed in dip kinematics ($\omega = 334$ MeV). The cross sections were measured for three electron kinematics (three virtual-photon polarizations) in both experiments. Although no Rosenbluth separation was reported for Florizone′s data, the author deduced the longitudinal/transverse behavior of the cross-sections, by removing their dependence on the off-shell electron-proton cross section, σ_{CC1} as prescribed by de Forest [30]. He concluded, that in quasi-elastic ^{4}He(e,e′p)^{3}H reaction, the longitudinal/transverse behavior of the cross section for missing momenta up to at least 90 MeV/c, is completely determined by σ_{CC1}, in disagreement with the conclusion of Ducret [10]. Not surprisingly, the data in the dip region by Kozlov does show a larger transverse than longitudinal spectral function by approximately 30 percent.

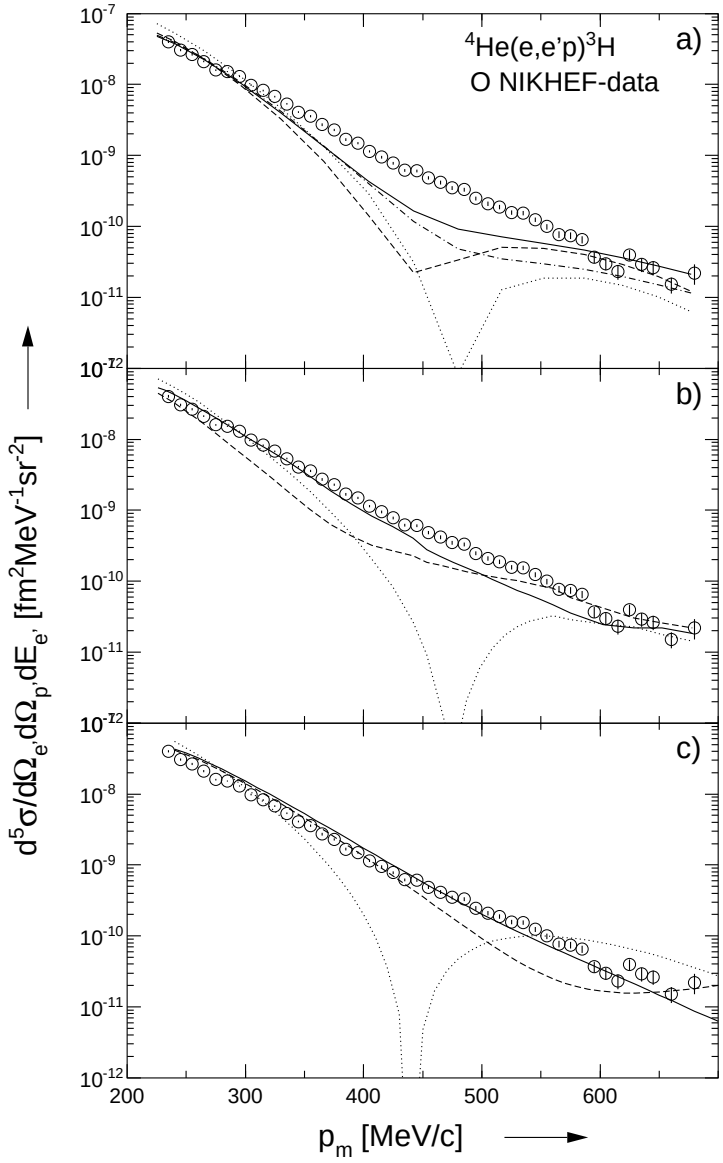

Fig. 2. Shown above are results from van Leeuwe *et al* [7]. The fivefold differential ^{4}He(e,e′p)^{3}H cross section as a function of the missing momentum for $\omega = 215$ MeV and $\mathbf{q} = 401$ MeV/c. The calculations in the top figure were performed by J.-M. Laget [22]. The dotted curve is the PWIA calculation, the dashed includes FSI, the dot-dashed includes two body MEC, and the solid includes three-body MEC. The calculations for the middle figure were performed by R. Schiavilla [17]. The dotted curve is the PWIA calculation, the dashed curve includes FSI, and the solid curve includes two-body currents. The calculations for the bottom figure were performed by S. Nagorny [23,24]. The dotted curve is the PWIA calculation, the dashed includes tree-type diagrams, and the solid includes one-loop diagrams.

There exist also several data sets for the semi-inclusive ^{4}He(e,e′p)pnn reaction, all at transferred momenta of a few hundreds MeV/c. For example, J.J. van Leeuwe *et al.* [6,31] measured the cross sections in dip kinematics (x_B=0.29) for at $Q^2 = 0.115$ (GeV/c)^2 at NIKHEF. The data are for missing energies up to 120 MeV, and missing momenta up to 600 MeV/c. They observe a large enhancement of the cross sections at high missing energies at increasing missing momenta. Comparing the data to calculations by Laget, the authors attribute this enhancement to two-body MEC and IC currents, as well as to short-range correlations which were explicitly included in Laget's wave function. Similar enhancement of the cross section at large missing energies for increasing missing momenta was observed by N. Liyanage *et al.* [32] in ^{16}O(e,e′p) data from Jefferson Lab at much higher momentum transfer, $Q^2 = 0.8$ (GeV/c)^2, for which calculations by Ryckebusch *et al.* [33] arrive at a similar conclusion.

Data from Saclay [34] in kinematics $0.4 < x_B < 1.8$ also note a peak in the missing energy spectra for various missing momenta, as shown in Fig. 3. In addition to becoming more pronounced as the missing momentum increases, the peak moves to higher missing energies with increased missing momenta. The location of the peak corresponds to the expected location of the correlated two-nucleon peak given by,

$$E_m \;=\; E_{thr} + \left(\frac{A-2}{A-1}\right)\frac{p_m^2}{2m_p} \tag{13}$$

where E_{thr} is the missing energy corresponding to the continuum threshold, p_m is the missing momentum, and m_p is the mass of the proton.

In MAMI, both Florizone [27] and Kozlov [28] measured the cross sections at high missing energies. They also studied the longitudinal/transverse behavior by integrating the cross-section over the measured range of missing momenta. In Florizone′s quasi-elastic kinematics, the L/T behavior follows that of σ_{CC1}, while at Kozlov's dip kinematics the transverse spectral function is increasingly larger than the longitudinal for increasing missing energies. Both data sets were compared to calculations by Efros *et al.* [20] which employ Lorentz integral transform method. For both missing energy spectra and continuum "distorted" momentum distributions the calculations agree reasonably well with both data sets, perhaps better with the quasi-elastic data of Florizone.

Again, it is useful here to mention the successfully completed experiment in Hall A on ^{3}He [35]. In this experiment, the ^{3}He(e,e′p) cross sections and response functions were measured for large transferred momenta. A detailed description of these measurements is given in Section 6.1. It is clear that the data are of very high quality and the challenge of response function separation at these kinematics can be met. It is important to note that our proposed measurement on ^{4}He will provide cross section and separated response functions in similar kinematics to those of the ^{3}He measurement. These data, in addition to their inherent value, will facilitate a very meaningful comparison between ^{3}He and ^{4}He in similar kinematics.

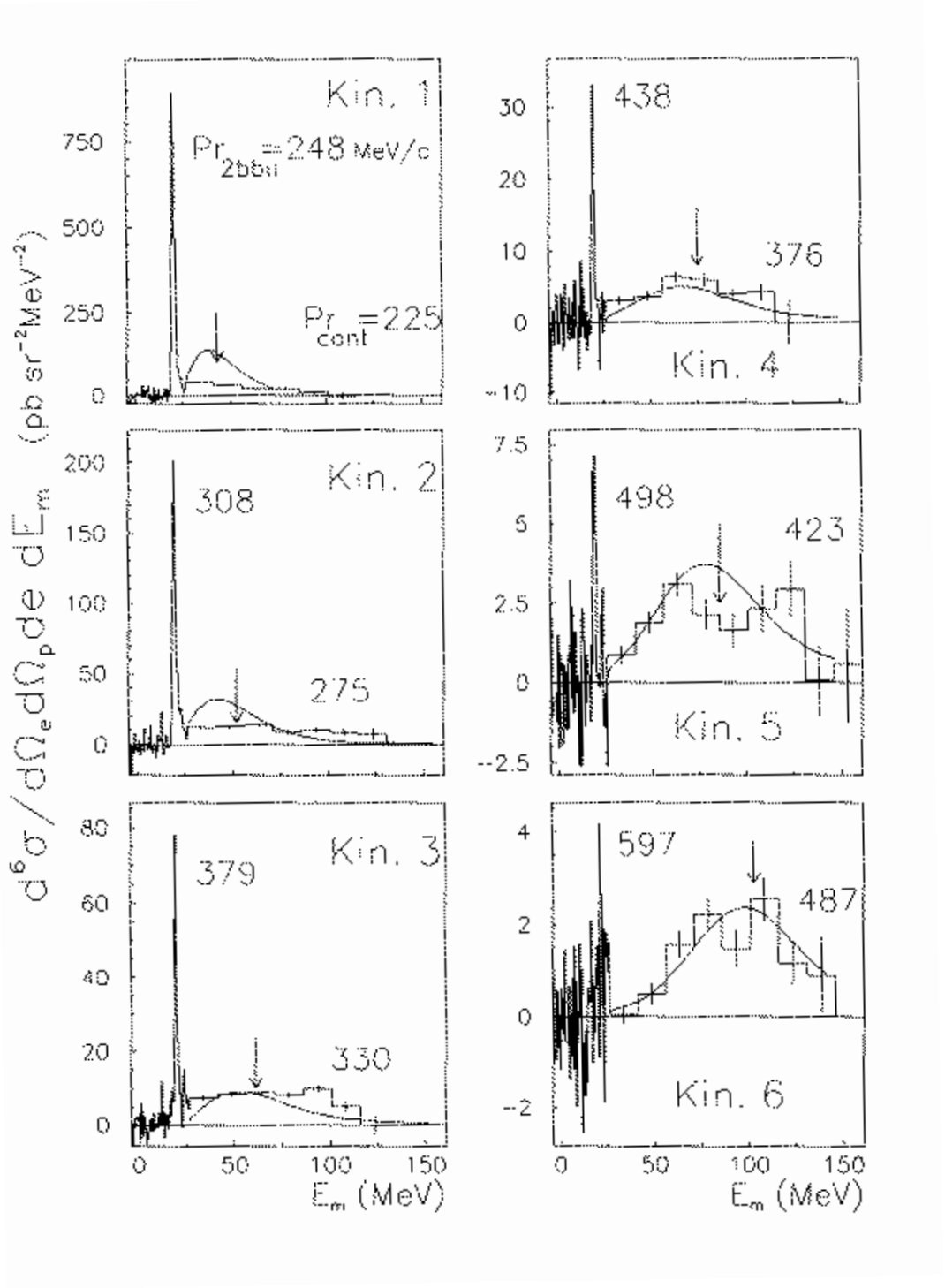

Fig. 3. Shown above the data from J.M. Le Goff *et al.* [34]. The radiatively corrected experimental cross section for various kinematics are shown as a function of missing energy, p_m. The arrow indicates where the nucleon-nucleon peak is expected. The curves are the result of a microscopic calculation by J.-M. Laget.

Polarization transfer measurements have been also used to extract the ratio (P'_x/P'_z) in the $(\vec{e}, e'\vec{p})$ reaction on helium. The first ^{4}He$(e, e'\vec{p})^3$H polarization-transfer measurements were performed at the Mainz microtron (MAMI) at $Q^2 = 0.4$ (GeV/c)^2 [36] and at Jefferson Lab Hall A at $Q^2 = 0.5$, 1.0, 1.6, and 2.6 (GeV/c)^2, E93-049 [37]. Our recent experiment E03-104 [38] extended these measurements with two high-precision points at $Q^2 = 0.8$ and 1.3 (GeV/c)^2. All these data were taken in quasielastic kinematics at low missing momentum with symmetry about the three-momentum-transfer direction to minimize conventional many-body effects in the reaction. The results are shown in Fig. 4 (solid points).

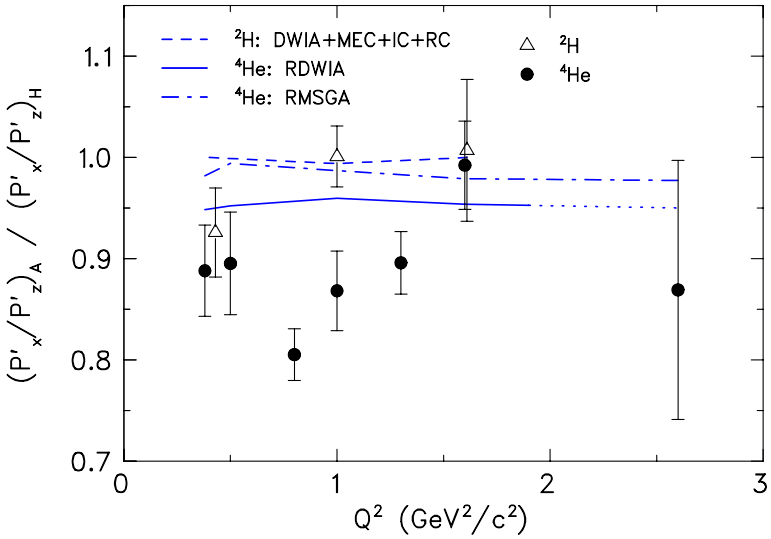

Fig. 4. Bound-to-free polarization-transfer double ralio R for ^{2}H($\vec{e}$,e'$\vec{p}$)n (open triangle) from [39] and for ^{4}He($\vec{e}$,e'$\vec{p}$)^{3}H (closed circles) from [36–38] as a function of Q^2. The curves show results of the calculation by Arenhovel (dashed line) for deuterium, a RDWIA calculation for helium by Udias *et al.* and a relativistic Glauber model calculation for helium by Lava *et al.* (dash-dotted line) [40]. While the deuterium data are consistent with the conventional model, the helium are not. The helium data from E03-104 at 0.7 and 1.3 (GeV/c)^2 are still preliminary and their final uncertainties are expected to be smaller [41]

5.4 Motivation for Perpendicular Kinematics

Perpendicular kinematics is suitable for measuring the cross sections up to very high missing momentum in constant electron kinematics (same transferred momentum **q** and energy ω). As such, it will be used in the separation of the longitudinal-transverse interference response, R_{TL}, and the asymmetry A_{TL} as well as in the extraction of the response R_T and a combination of the longitudinal and transverse-transverse interference responses R_{L+TT}. All variables will be measured up to large p_m.

It is very useful to think of ^4He both as a few-body system and as a complex nucleus. Spectral functions for ^4He have been calculated both microscopically and in mean-field frameworks. Similarly, the $^4He(e, e'p)$ reaction dynamics has been calculated in both frame-

works. As a consequence, measurements of cross sections and cross-section type response functions can be examined from both points of view, enabling the consolidation of model predictions for nuclei ranging from the deuteron to ^{16}O and possibly even Pb.

We already obtained recent predictions for the measured $^4He(e,e'p)^3H$ cross section for the missing momentum range $0 \leq 1.0$ GeV/c calculated several ways: microscopically using the diagrammatic approach by Laget, using RDWIA by the Madrid group, and handling FSI by the Eikonal approximation by Ryckebusch. These cross sections, at quasielastic kinematics are sensitive to both the spectral function and reaction dynamics effects such as FSI. Similar calculations by Laget and the Madrid group have been compared also to our recent similar data for $^3He(e,e'p)^2H$ with impressive success. They indicate that for the $^3He(e,e'p)^2H$ reaction, FSI dominates the cross section for $250 \leq p_m \leq 650$ MeV/c; for lower p_m, the FSI are small and the cross section is very sensitive to the ground-state wave function while for p_m above 700 MeV/c, the cross section is surprisingly large and can be quantitatively described by the models only by invoking double-scattering FSI. It is possible, that non-nucleonic degrees of freedom are required for a more quantitative description of the data for p_m above 700 MeV/c. Two additional models, by Ciofi degli Atti [42,43] and Sciavilla [44], were also used to calculate the $^3He(e,e'p)^2H$ reaction with great success. All models can perform similar calculations for $^4He(e,e'p)^3H$, which we expect upon obtaining the data.

In contrast to ^3He which is a loosely-bound nucleus, ^4He is tightly bound and much more dense, and hence the comparison between the two nuclei will yield very valuable information on the dependence of the spectral function, reaction dynamics and the onset of partonic degrees of freedom on the nuclear density. To help disentangling gswf from reaction dynamic effects, we shall measure the A_{LT} asymmetry up to p_m 0.5 GeV/c. For ^3He, all models indicate that factorization is broken by interference between the plane wave and re-scattering amplitudes, resulting in an A_{LT} shape typical of broken factorization. Similar calculations by the Madrid group of the A_{TL} asymmetry for the $^{16}O(e,e'p)^{15}N$ reaction that reproduce the data very well indicated broken factorization due to relativistic dynamical effects by enhancement of the lower components [8]. For the case of ^{4}He, the Madrid group predicts a very large A_{TL} asymmetry due to both the relativistic dynamical effects as in ^{16}O and the interference of the plane-wave and re-scattering amplitude as in ^{3}He, while the Laget model predicts a significant but smaller A_{TL} asymmetry due entirely to the interfering amplitudes as in ^3He. The proposed measurement will undoubtedly resolve the difference between these very different approaches, as well as with other models, each predicting a slightly different A_{TL} resulting from the difference in the model ingredients.

For missing momentum p_m between 0.325 GeV/c to 0.575 GeV/c, we propose to measure the cross section at a second electron angle but at the same transferred momentum and energy. This will allow the extraction of R_T and R_{L+TT} by Rosenbluth separation for this range of missing momenta. We note that most models predict a minimum in the proton-triton momentum distribution at $p_m = 425$ MeV/c, which has not been observed for low or high transferred momenta in either perpendicular or parallel kinematics [7,9].

The diagrammatic model by Laget predicts that this minimum will be observed in the R_{L+TT} response. In any case, the availability of the cross section, R_{TL}, A_{TL}, R_T and R_{L+TT} for this p_m range will greatly constrain the ingredients in all available models.

5.5 Motivation for Parallel Kinematics

We propose to extract the longitudinal and transverse response functions for several transferred momenta, $\mathbf{q} = 1$, 1.5, 2, 3 GeV/c, by performing a Rosenbluth separation in quasielastic parallel kinematics. The measurements will be done for low missing momenta. Ducret *et al.* [10] observed a quenched longitudinal response at $Q^2 < 0.6$ (GeV/c)^2, which they attributed to modification of the nucleon form factor in the dense ^{4}He medium. It will be very interesting to investigate the evolution of this effect with momentum transfer. Again, the high transferred momentum allows the use of the Eikonal approximation for treatment of the final-state interactions. The use of parallel kinematic will also help in minimizing the effects of FSI. A sample of the cross section results in forward parallel kinematics in the E89-044 experiment for Q^2 up to 4 (GeV/c)^2 is shown in Figure 5. One can see that FSI contributions are small.

The data will be compared to similar data obtained for ^{3}He in the same kinematics [35], allowing for a unique study of density effects. We note that these measurements are proposed where the cross sections are very high, and the beam-time required is small, providing a very favorable cost-benefit balance for this measurement.

We propose also to extract the longitudinal and transverse response functions in non-quasielastic anti-parallel kinematics for missing momentum, $p_m = 0.4$ GeV/c, for the reaction ^{4}He(e,e′p)X. The R_L and R_T responses will be measured The measurement will be done for transferred momenta of 1.5 GeV/c. Again, with this high transferred momentum, and especially for anti-parallel kinematics, we expect the FSI to be under theoretical control. Also for the anti-parallel, $x_B = 1.86$, we expect two-body currents to be highly suppressed and predominantly transverse, while short-range nucleon-nucleon correlations are predicted to be observed [13] and predominantly longitudinal.

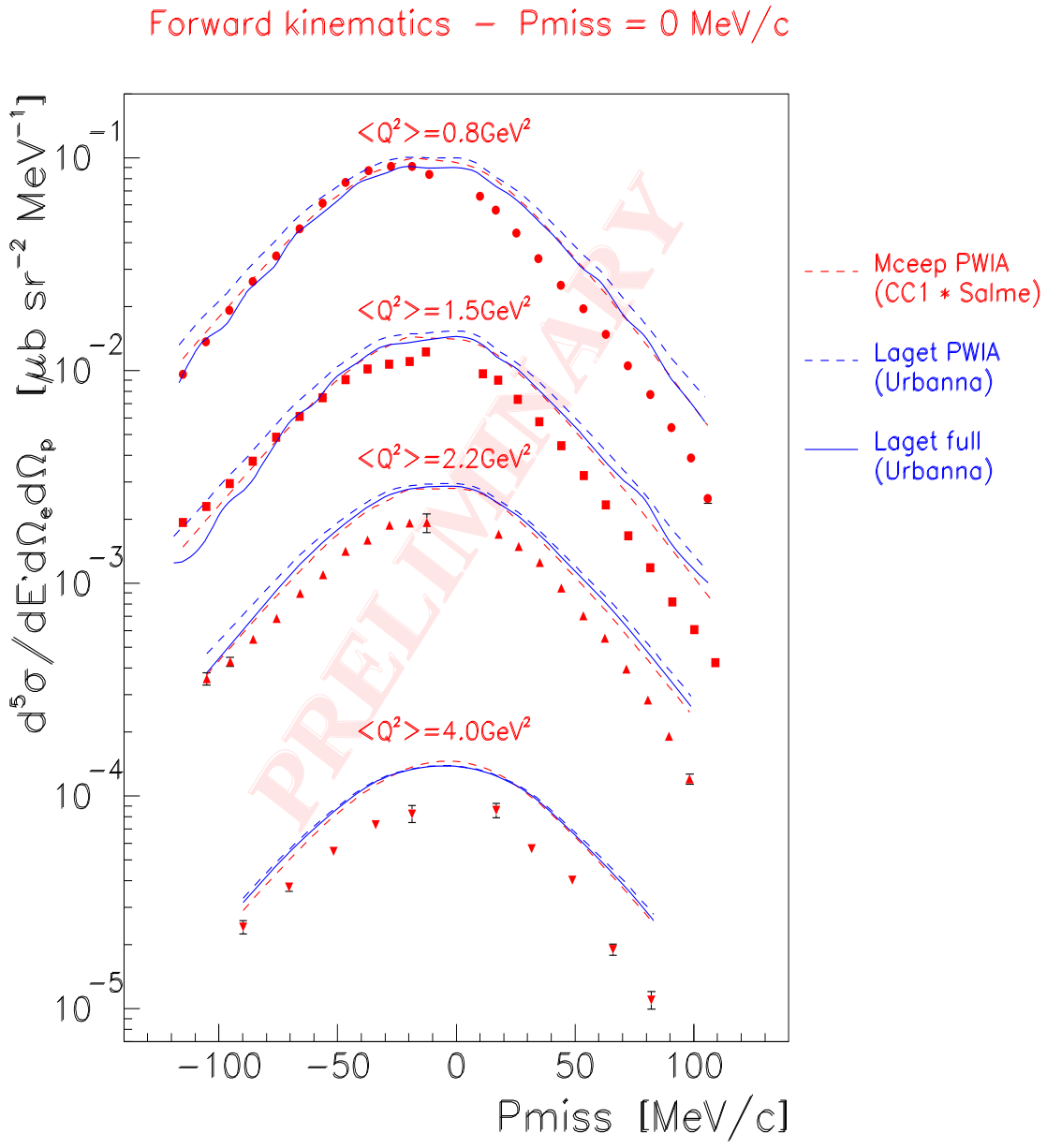

Fig. 5. Shown is the ^{3}He(e,e′p)d cross section results from the E89-044 parallel kinematics analysis at $p_m = 0$ and Q^2 up to 4 (GeV/c)^2. Similar statistics are expected for our proposal on ^{4}He(e,e′p)^{3}H.

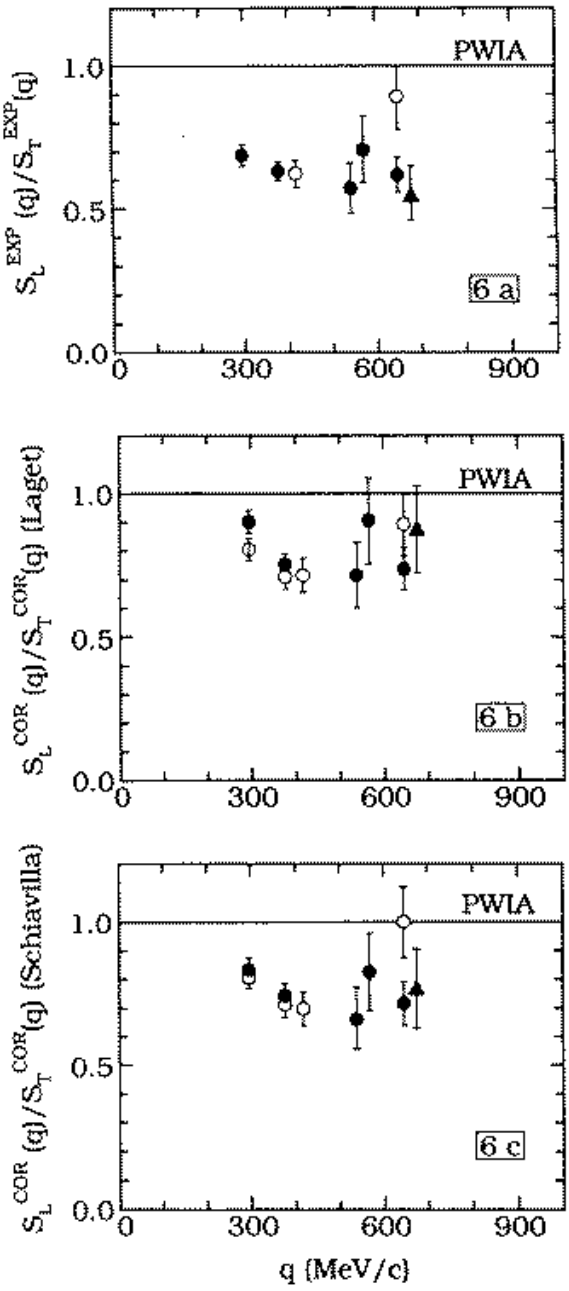

Fig. 6. The data of Ducret *et al* [10]. The ratio of longitudinal to transverse spectral functions as a function of momentum transfer **q**. Open circles correspond to $p_m = 30$ MeV/c, the solid circles correspond to $p_m = 90$ MeV/c, and the solid triangles correspond to $p_m = 190$ MeV/c. The horizontal lines indicate the PWIA ratio. In upper most plot, the experimental spectral functions S_L^{EXP}/S_T^{EXP} is shown, in the middle plot the ratio of the spectral functions is shown with correction factors from J.-M. Laget [26], and in the bottom figure the ratio of the spectral functions is shown with correction factors from R. Schiavilla [18].

6 Relation to other Jefferson Lab Proposals

6.1 Hall A Experiment 89-044

The aim of this experimental program was to investigate three specific aspects of the electromagnetic response of ^{3}He through (e,e′p) coincidence measurements. In perpendicular kinematics, with a constant $\mathbf{q} = 1.5$ GeV/c and $\omega = 0.845$ GeV, the single nucleon structure of ^{3}He was studied with special emphasis on high momenta, up to 1 GeV/c in missing momentum.

We also did a complete in-plane separation of the response functions R_{TL}, R_T, and the combination of R_{L+TT} up to missing momenta of 0.55 GeV/c. In parallel kinematics, the $\mathbf{q}$ dependence of the reaction was determined by performing an R_L/R_T (longitudinal/transverse) Rosenbluth separation for protons emitted along $\mathbf{q}$ (in parallel kinematics), up to $\mathbf{q} = 3$ GeV/c. This was performed in both quasifree kinematics ($p_m = 0$) and for q = 1 and 2 GeV/c at $p_m \pm 0.3$ GeV/c. Also, the continuum region was studied in order to search for correlated nucleon pairs. This was done in both parallel and perpendicular kinematics with full in-plane separation of the response functions.

For the present proposal on ^{4}He we have decided to use the same kinematic conditions, $\mathbf{q} = 1.5$ GeV/c and $\omega = 0.84$ GeV, as was used for the ^{3}He experiment. Based on discussions with theorist, such as R. Schiavilla and S. Jeschonnek, it is clear this choice of kinematics will facilitate a comparison of the data from ^{4}He and ^{3}He.

Shown in Fig. 7 are the high epilson ^{3}He(e,e′p)d data for the right and left side of the $\mathbf{q}$ vector. Figure 8 displays the extracted A_{TL} data with the PWIA and full calculations using two ground-state wave functions. The difference in the two ground-state wave functions has a very small effect in the full calculations. In contrast to the PWIA calculations, the measured A_{TL} displays a structure characteristic of broken factorization [45]: the oscillating pattern of A_{TL} comes directly from the interference between different reaction amplitudes. Both full calculations describe the data reasonably well by displaying similar structure. Such structure in A_{TL} was previously observed in the quasielastic removal of p-shell protons in the ^{16}O(e,e′p) reaction [8], and was well reproduced by relativistic Distorted-Wave Impulse Approximation calculations by Udias *et al.* [46]. In that case broken factorization was attributed to dynamical relativistic effects, enhancement of the lower components of the Dirac spinors. However, these effects are marginal in our experiment because of the low nuclear density of ^{3}He [47]. Rather, in our case the factorization is broken by the strong interference between the PWIA and re-scattering amplitudes [48]. ^{4}He is expected to be the bridge nucleus between the high and few-body nuclei where the mean field calculation and microscopic calculations come to near agreement.

Figure 9 shows some of the many continuum results that were extracted from the E89-044 data. Figure 10 shows a comparison between the proton effetcive momentum density distribution for the two body breakup and the continuum channels [1]. The present

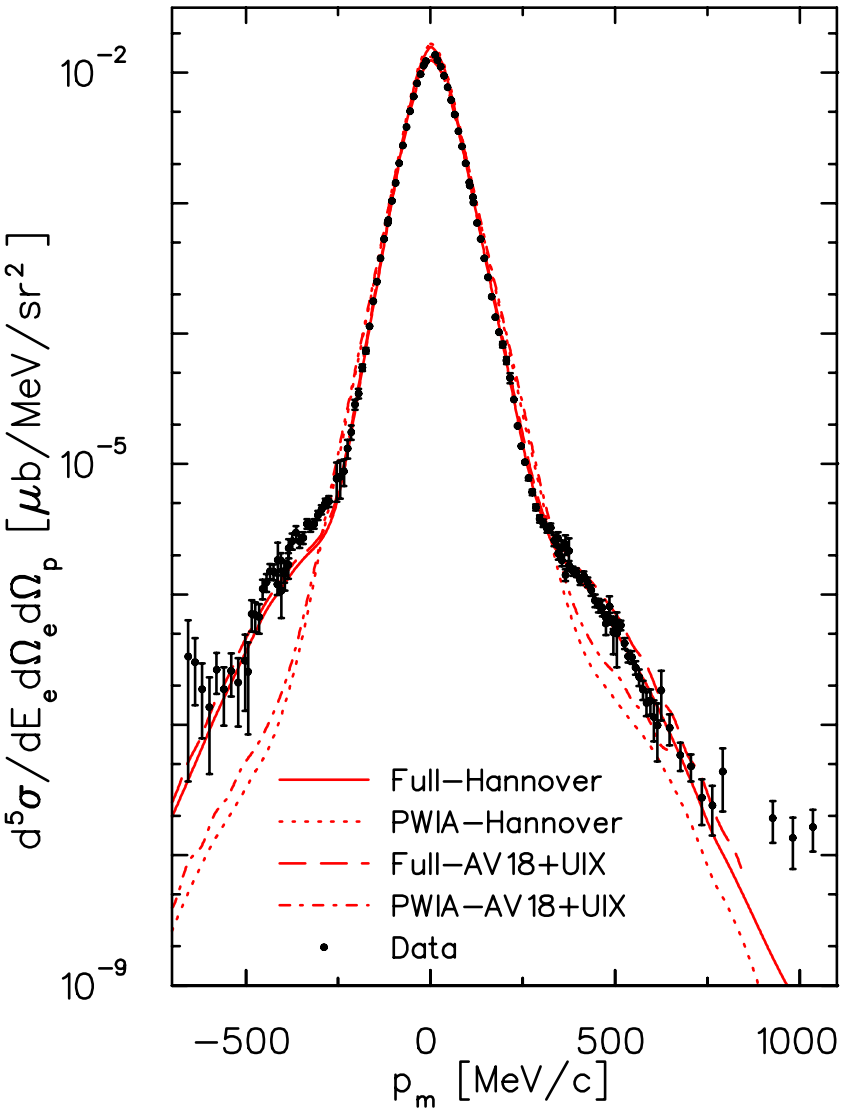

Fig. 7. Shown are the ^{3}He(e,e′p)d results of experiment E89-044 at high epsilon, $\mathbf{q} = 1.5$ GeV/c, and $\omega = 0.845$ GeV for the right and left side of the momentum transfer vector. From this result alone, one can see that the data are described at low missing momentum by calculations using modern three body wavefunctions and plane-wave impluse approximation, at high missing momenta the inclusion of final state interactions becomes critical and at the highest missing momentum there are effects which are not yet well understood. The difference over the sum of these results, A_{LT}, is shown in Fig. 8.

proposal will provide data of similar quality for ^{4}He on both the two-body break-up channel and for the continuum.

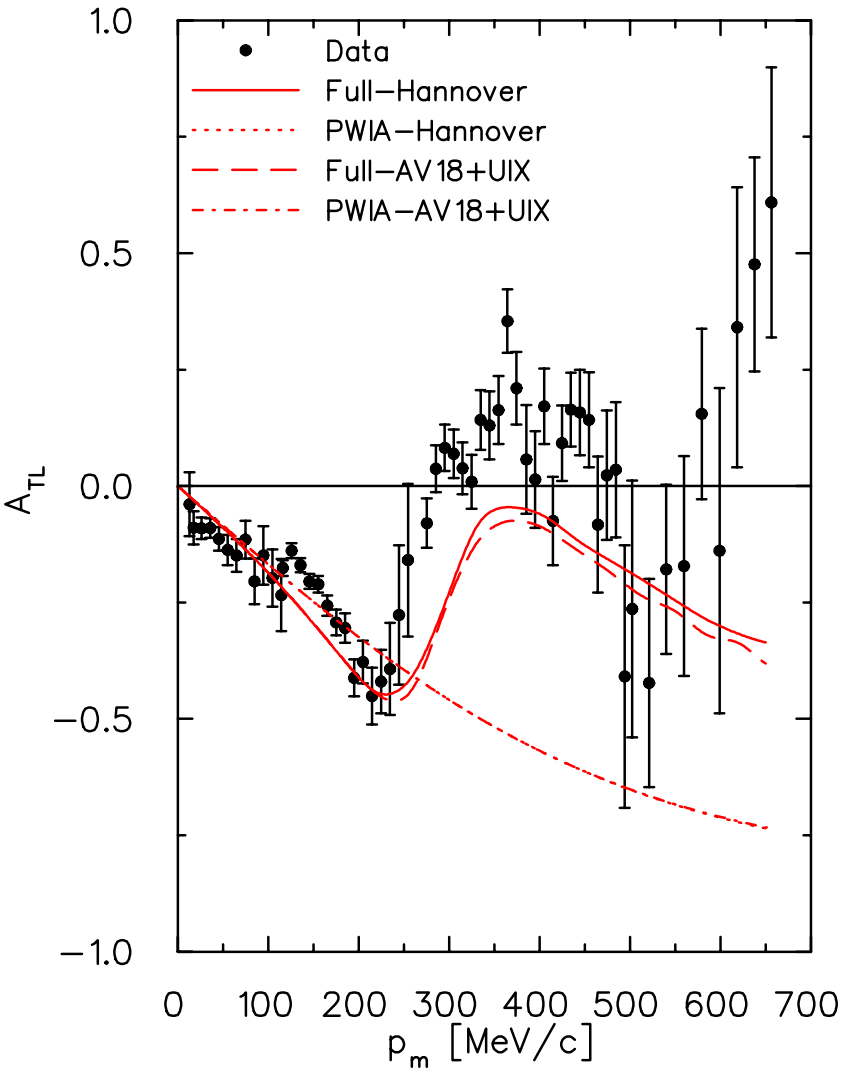

Fig. 8. Shown is the A_{LT} asymmetry formed from the data shown in the previous figure.

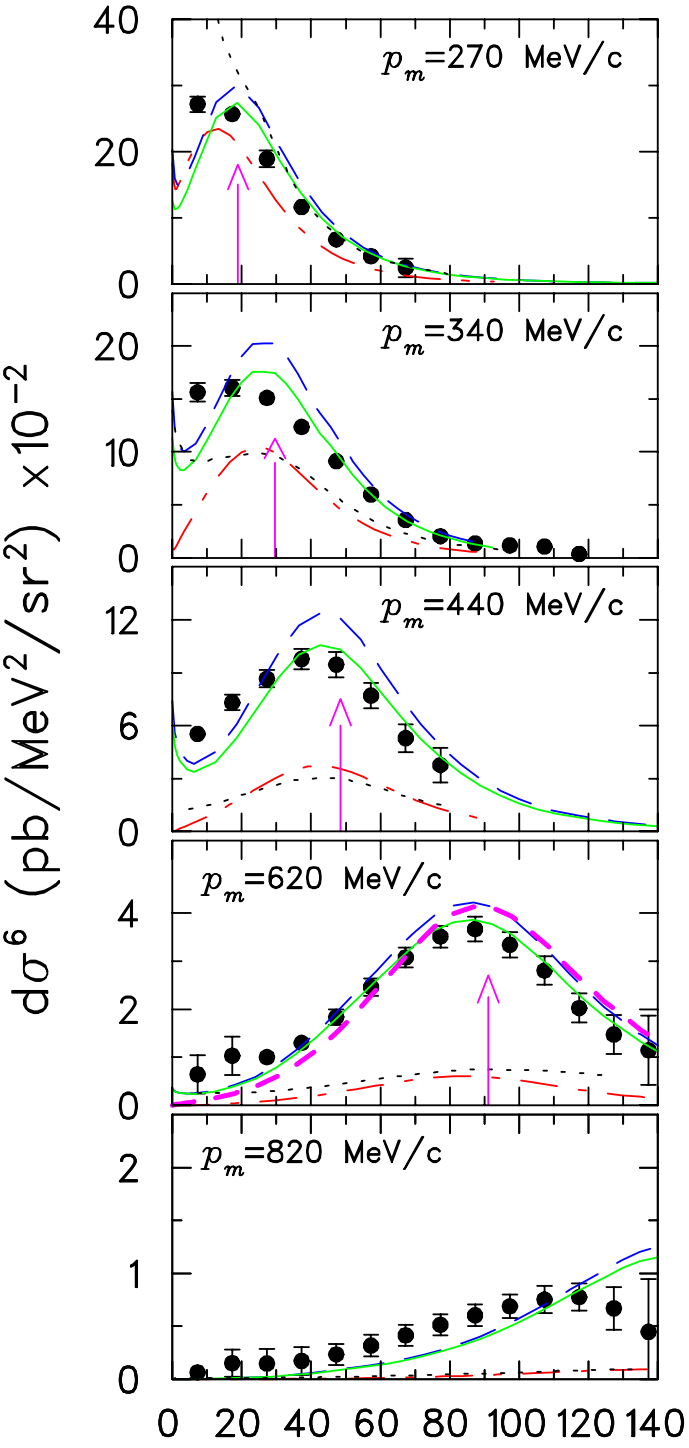

Fig. 9. Cross-section results for the ^{3}He(e, e′p)pn reaction versus missing energy E_m. The vertical arrow gives the peak position expected for disintegration of correlated pairs. The dotted curve presents a PWIA calculation using Salme's spectral function and σ_{cc1} electron-proton off-shell cross section.Other curves are theoretical predictions of J.-M. Laget from the PWIA (dash dot) to PWIA + FSI (long dash) to full calculation (solid), including meson exchange current and final state interactions. In the 620 MeV/c panel, the additional short dash curve is a calculation with PWIA + FSI only within the correlated pair. This same quality of continuum data will be obtained during this proposed ^{4}He experiment.

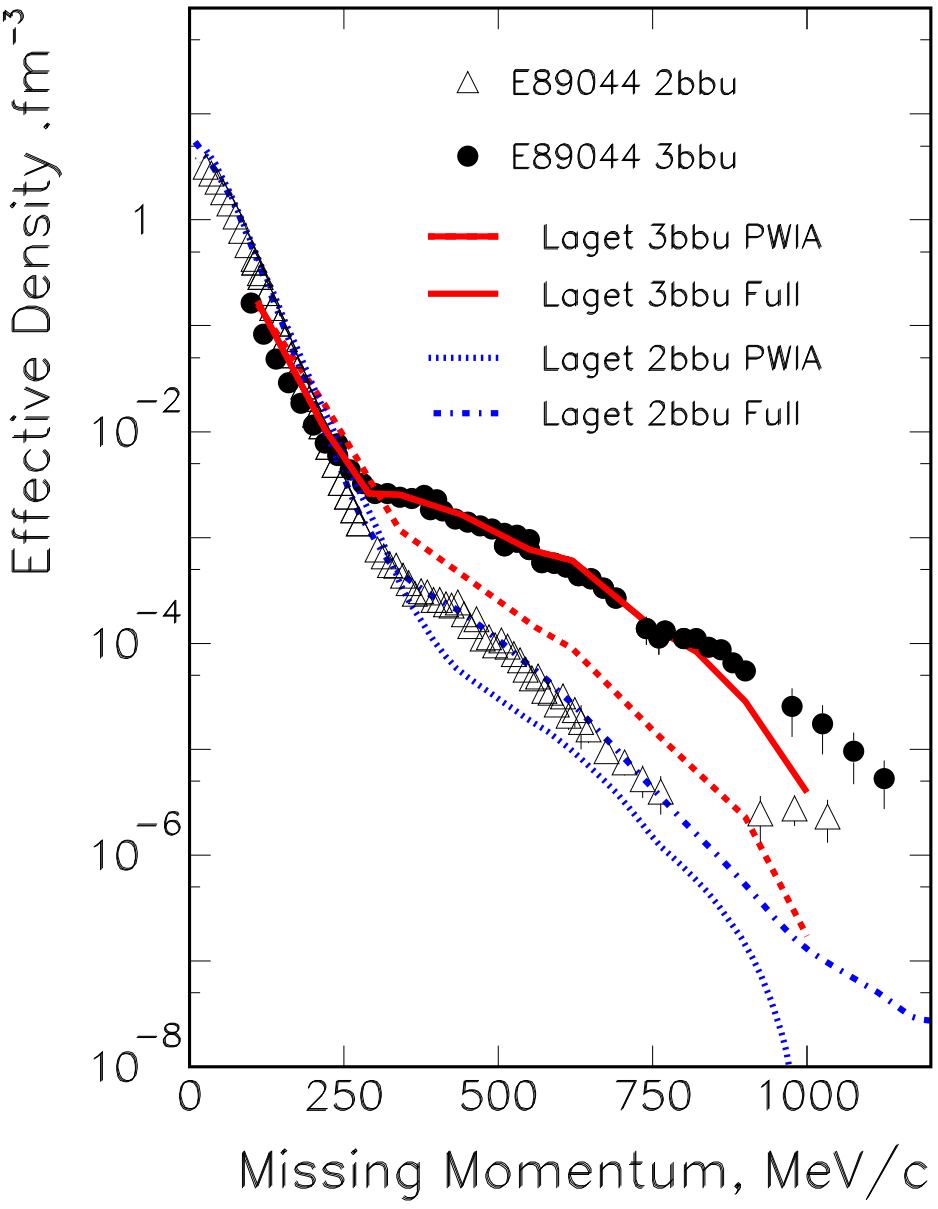

Fig. 10. Proton effective momentum density distributions in ^{3}He extracted from ^{3}He(e,e′p)pn (black points) and ^{3}He(e,e′p)d (open triangles) from the E89-044 experiment [1] for perpendicular forward kinematics, compared to calculations from J.M. Laget. The 3bbu integration covers E_M from threshold to 140 MeV.

6.2 Hall A Experiment 97-111

Data collection for this approved experiment was completed in Fall, 2000. The aim of this proposal was to measure cross sections for the ^{4}He(e,e′p)^{3}H reaction in a range of missing momenta which spanned the theoretically predicted minimum at $p_m = 0.425$ GeV/c. The depth of the minimum in the cross section reflects the minimum in the spectral function for the triton ground state transition. The minimum is expected to be clearly seen if the Plane Wave Impulse Approximation is valid. Meson exchange currents and final state interactions tend to fill the minimum in the cross section. E97-111 was performed for two settings of constant q-ω which gave a kinetic energy of the proton in the triton's rest frame of 0.345 GeV. In the proposed experiment for perpendicular kinematics we will maintain a kinetic energy of the proton in the triton's rest frame of 0.809 GeV. At this higher energy the final state interactions can be treated using either the generalized Glauber approximation, or by an optical potential. E97-111 also measured in parallel kinematics for the positive y configuration ($\cos(\theta_{qx}) = -1$.) in two settings. For both kinematics missing momenta up to 0.5 GeV/c were investigated. No separations of response functions were attempted in E97-111, whereas this is part of the goal of the current proposal. The preliminary result of this experiment E97-111 can be seen in Fig. 11.

6.3 Hall B Experiment 89-027/91-009

Measurements were made using the CLAS on ^{3}He, ^{4}He, ^{12}C and ^{56}Fe with 1.1, 2.2 and 4.4 GeV electrons in 1999 with polarized beam [49,50] (Measurements were not made on ^{4}He at 1.1 GeV.) There is no real overlap between these data and our proposed measurement. The CLAS experiment measures a far greater kinematic range (in Q^2 and ω) than this Hall A proposal, can measure the out-of-plane response functions in some kinematics and can measure 2 (or more) nucleon knockout; but in order to do this, they need to integrate over a significantly larger Q^2 and ω bin than we will measure. The CLAS is very well suited for surveys of the dominant reaction channels. However, for detailed studies of specific reaction channels in extreme kinematical conditions, the high luminosity, high resolution Hall A spectrometers are the optimal choice.

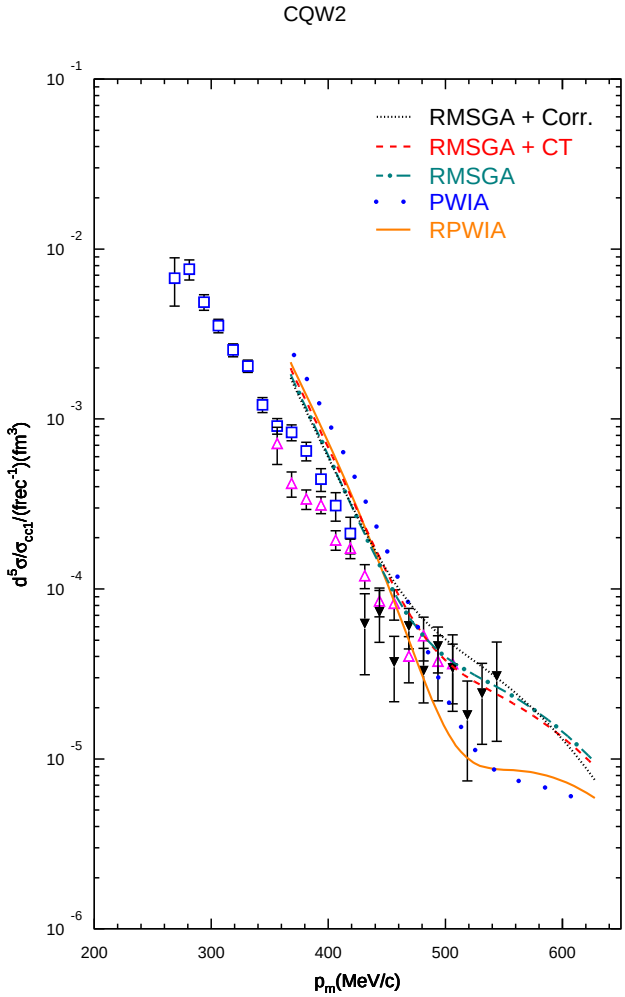

Fig. 11. Shown is a preliminary cross section result from experiment E97-111 along with calculations from J. Ryckebusch. While in 1997 when this experiment was proposed, it was thought that the dip would be clearly visable; modern calculations (including this one) show the dip is filled in. This experiment will further explore this region by not only measuring cross section; but also, response functions and the A_{LT} asymmetry.

7 Theoretical Predictions

7.1 Relativistic Mean Field Calculation

In the relativistic mean field calculations performed with the code provided by J.M. Udias [51], a bound state wave function is used that is the solution of the Dirac equation using standard Wood-Saxon (WS) wells for the scalar(S) and vector(V) potentials. The parameters of the WS potentials are fitted to the measured rms radius and binding energy of ^{4}He. This reproduces quite well the ^{4}He(e,e′p)^{3}H momentum distribution. A general solution of a bound particle using the Dirac equation has a different ratio of upper and lower components than for a free nucleon, that is, it always has a negative energy component. The spinors in a completely relativistic calculation are often referred to as "distorted" because of the presence of the scalar and vector potentials appearing in the lower component [19,52]. The positive energy projected solutions resemble free spinors containing only the usual terms connecting the upper and lower components, The Udias code calculates DWIA or PWIA always using relativistic kinematics. Proton distortions are calculated solving the Dirac equation using an optical potential. The only nonrelativistic option is to remove the relativistic dynamics from the wave functions, for either the bound state proton or continuum proton, by projecting out the negative energy components, but the operator and kinematics will still be fully relativistic. It is worth noting that the recent Hall A results for response functions and the A_{TL} asymmetry from ^{16}O(e,e′p)^{15}N [8] were well described by the full relativistic calculation of Udias [46,53].

7.2 Microscopic Calculation

In the microscopic calculation performed with a code provided by J.-M. Laget, the reaction amplitude is expanded in diagrams which are computed in momentum space [22]. The code used the Urbana V14 potential. The diagrams for his Plane Wave Impuse Approximation, PWIA, calculation are shown in Fig. 12. The left diagram is the simplest Feynman diagram for the ^{4}He(e,e′p)^{3}H reaction. In this figure the virtual photon couples to one-nucleon. In the right diagram, the recoil contribution is taken into account, i.e. when the virtual photon couples to the triton.

For the full calculations of J.-M. Laget, the two-body and three-body mechanisms are taken into account. The two-body diagrams are shown in Fig. 13. Here the two-nucleon meson exchange amplitudes are shown in a. and b. and the nucleon-nucleon rescattering is taken into account in diagrams c. and d. Both isospin states (T=0,1) of the initial nucleon pair are taken into account. Three-body diagrams are shown in Fig. 14. In these diagrams the recombination of the ^{4}He breakup and the ^{3}H recombination are taken into account.

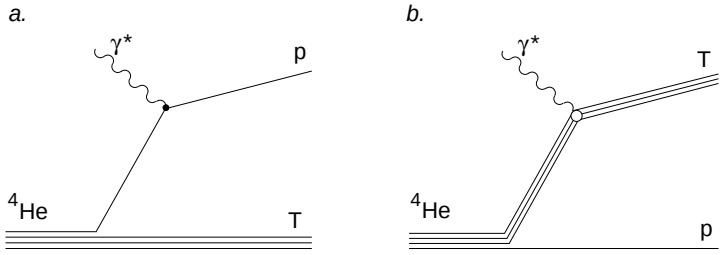

Fig. 12. The one-body mechanisms.

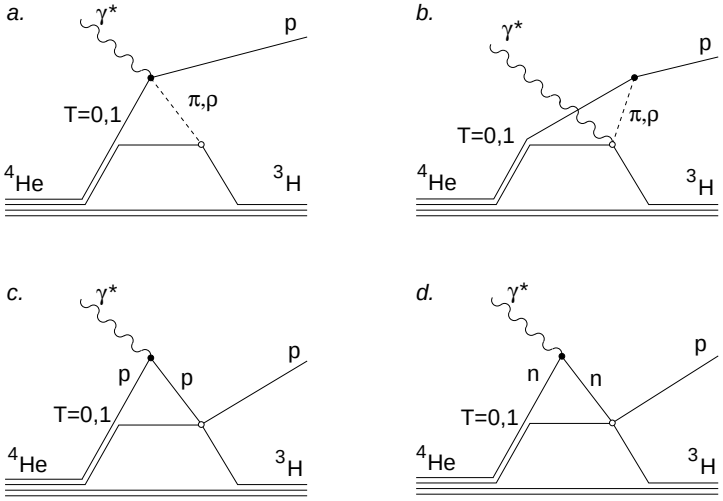

Fig. 13. The two-body mechanisms.

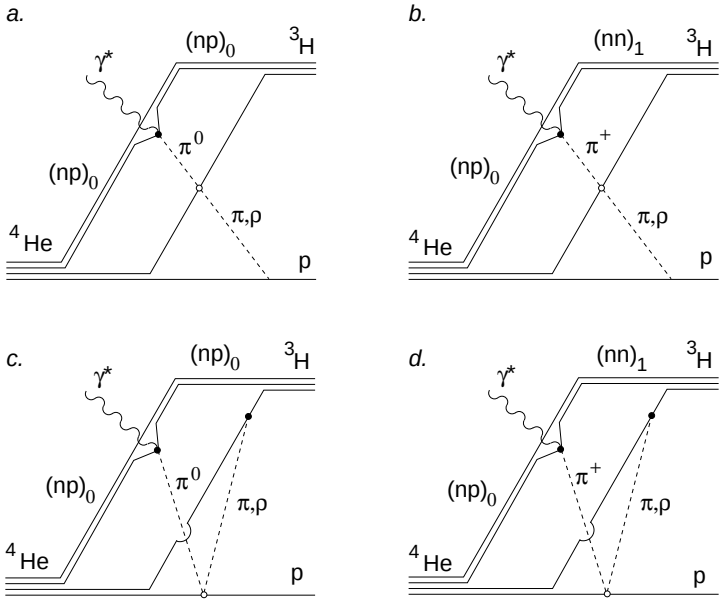

Fig. 14. The three-body mechanisms.

7.3 Other Theoretical Developments

J. Ryckebusch *et al.* [54] have developed a method of comparing optical potentials to Glauber type calculations in a real systematic way. The results of Ryckebusch's calcutions are shown compared to the E97-111 data in section 6.2 and, as can be seen in Fig. 15, these calculations have also been applied to the proposed kinematics.

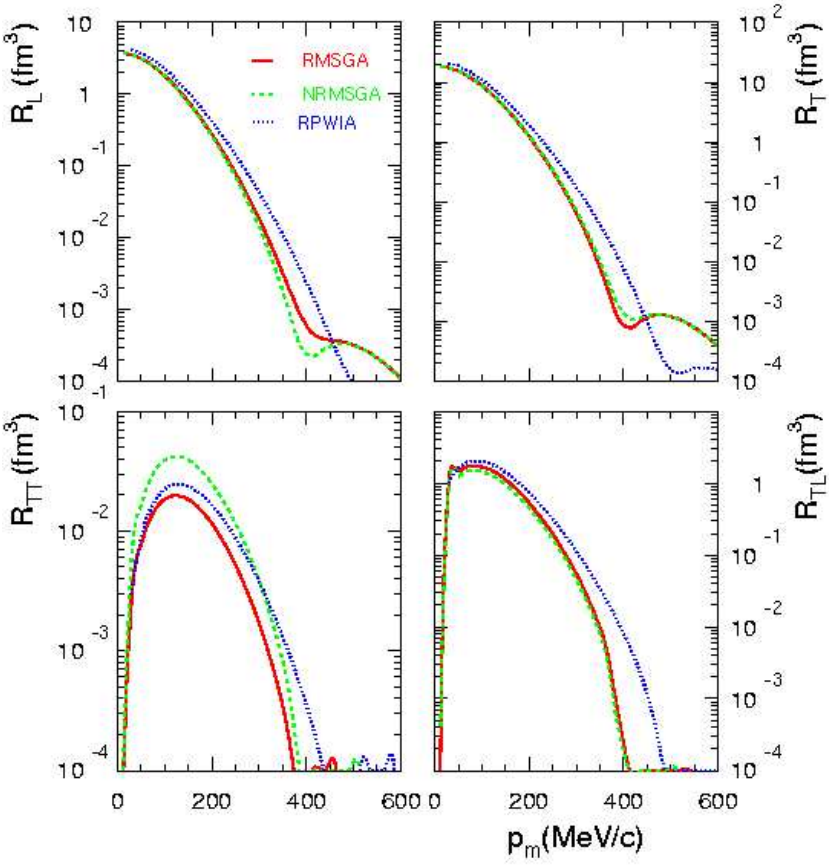

Fig. 15. Shown is J. Ryckebusch *et al.* [54] prediction the separated ^{4}He response functions versus missing momentum for the constant ($\mathbf{q}$,ω) kinematics proposed herein.

C. Ciofi degli Atti *et al.* are now able to do calculations for both ^{3}He and ^{4}He within the same theoretical framework. These calculations have already been provide for the E89-044 ^{3}He experiment and the E97-111 ^{4}He experiment and Ciofi has joined this proposal and will provide his calculation for this experiment.

S. Jeschonnek and R. Schiavilla are developing detailed calculations for ^{3}He and ^{4}He [55]. R. Schiavilla will provide the bound state wave function using the Argonne V18 potential [56] while S. Jeschonnek will introduce the relativistic current operator, as she has already done for the deuteron [57]. This operator can now be applied to any target nucleus [55]. S. Jeschonnek will also include Final State interactions with the Glauber approximation [58]. When combined, this should provide the most realistic theoretical model for the recent ^{3}He(e,e′p) experiment and for this proposed ^{4}He(e,e′p) measurement.

8 Experimental Setup

Hall A has proven itself capable of extracting high quality response functions. We plan to measure the reaction (e,e′p) in ^{4}He, by making use of the techniques developed from the previous (e,e′p), [8,32,1,2,4] experiments. This experiment will use the Hall A high resolution spectrometers, and the cryogenic high pressure ^{4}He target. With a missing energy resolution of 1 Mev, the two-body peak, located at 19.8 MeV, will be well separated from the three- and four-body break-up continuum which start at 26.1 MeV and 28.3 MeV respectively.

Cross sections, count rate calculations, and simulations for the proposed measurements were estimated using a beam current of 75 uA on a 10 cm long "tuna can" ^{4}He cryogenic target with a density of 0.14 g/cm^3. This translates to a target luminosity of 1×10^{38} cm^{-2} sec^{-1}. A 20 cm long ^{4}He cryotarget, which has been built for the completed ^{4}He parity experiment, could double the proposed target luminosity for the back angle kinematics where we are not count rate limited. Since this new target cell is narrower, it would have the additional benefit of reducing the multiple scattering of the ejected particles, thus resulting in a better missing energy resolution.

The standard properties of the Hall A spectrometers were used in making the count rate estimates: solid angles of 5 msr and momentum bites of +/- 4.5%. We used a spectral function $S(p_m)$ which we parametrized from existing data on ^{4}He. In the low p_m region (0-200 MeV/c) we used the spectral function determined from the Mainz [59,27] and NIKHEF [60] data. Above 200 MeV/c we parametrized the spectral function data of van Leeuwe *et al.* [6,7] with an exponential fit. The resulting parameterization of the spectral function is shown in Fig. 16. We believe using this parameterization of the spectral function extracted from experimental data for the determination the ^{4}He(e,e′p)^{3}H cross sections is more realistic than using any determined from the various models. Also shown in the figure is the triton-proton momentum distribution obtained with the Argonne V18l [56] wavefunctions normalized to the same value of the integral as the experimental parameterization.

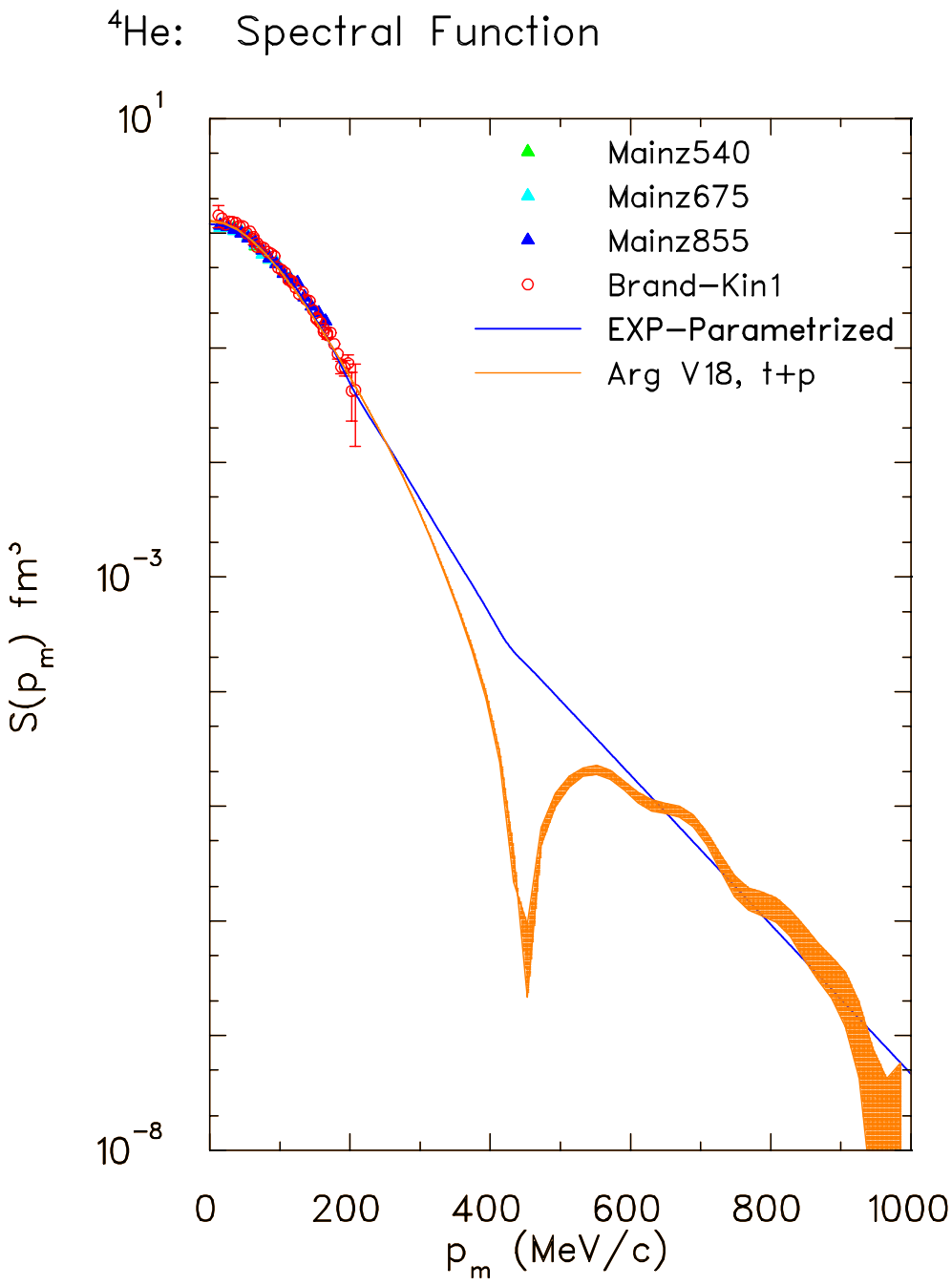

Fig. 16. Shown above is the parameterization of the ^{4}He spectral function. Also shown is the momentum distribution obtained from the Argonne V18 wavefunctions normalized to the same value of the integral as the experimental parameterization.

8.1 Proposed Kinematics

In the perpendicular kinematics, shown in Table 1, q will be fixed to 1.50 GeV/c and ω will be fixed to 0.837 GeV. With this constraint, the (e,e′p) cross section will first be measured with a beam energy of 4.80 GeV with proton detected on either side of the q-vector. This will allow the extraction of the R_{TL} response function and the A_{TL} asymmetry. Using a different beam energy, we measure the cross section for a p_m around zero, 0.400, and 0.500 GeV/c at a different epsilon. This will allow the extraction of the R_{L+TT} and R_T response functions. The final few kinematics will extend our knowledge of the ^{4}He(e,e′p) cross section to a $p_m = 1.2$ GeV/c.

In Table 2 the high missing momentum kinematics are shown. From the recent Hall A ^{3}He(e,e′p)d results, we expect the strength in the cross section as a function of missing momentum to be much higher than presently predicted. We are therefore requesting time to measure to as large a values of p_m as possible.

In parallel kinematics, shown in Table 3 and 4, the detected proton is emitted in the direction defined by the q-vector. With this constraint, the (e,e′p) cross section will be measured for a number of different transferred momenta and with different epsilon values. This will allow the extraction of the R_L and R_T response functions as a function of transferred momentum. These kinematics can be broken into two parts. The first is the low p_m high $\mathbf{q}$ to investigate the quenching of the longitudinal response function. The second is the high p_m points to investigate nucleon-nucleon correlations by making ^{4}He(e,e′p)pnn measurements in anti-parallel kinematics.

8.2 Singles Rates

The single-arm background rates is shown for the perpendicular kinematics in Table 5, for the high missing momentum in Table 6, and for parallel kinematics in Tables 7 and 8. The (e,e′p) rate were calculated with the QFS computer code and the (e,p),(e,π^+), and (e,π^-) rates were calculated with the EPC code of Lightbody and O'Connell [61]. The rates were calculated for a luminosity of 1.0×10^{38} cm^2/s. As demonstrated during the E89-044 ^{3}He(e,e′p) experiment, which made measurements in similar kinematics, rates such as these are not a problem for the Hall A spectrometers.

8.3 Coincidence Rates

We determined the coincidence rates by assuming a luminosity of 1×10^{38} cm^{-2} sec^{-1}. A missing energy width of 1.6 MeV and a timing width of 2 ns was used to determine the true and accidental rates. The computer code SEEX [62] was used in computing the fivefold differential cross sections (denoted as $\sigma 5$ in the tables) at each kinematic point.

Table 1
Perpendicular Kinematics

Kinematics	$\mathbf{q}$ [GeV/c]	E_o [GeV]	ω [GeV]	ϵ	E_e [GeV]	θ_e [deg.]	P_p [GeV]	θ_p [deg.]	p_m [GeV/c]
Kin01	1.50	4.80	0.840	0.943	3.96	16.4	1.49	48.2	0.000
Kin02	1.50	1.25	0.840	0.101	0.41	120.	1.49	13.6	0.000
Kin03	1.50	4.80	0.840	0.943	3.96	16.4	1.49	52.0	0.100
Kin04	1.50	4.80	0.840	0.943	3.96	16.4	1.49	44.4	0.100
Kin05	1.50	4.80	0.840	0.943	3.96	16.4	1.48	55.8	0.200
Kin06	1.50	4.80	0.840	0.943	3.96	16.4	1.48	40.5	0.200
Kin07	1.50	4.80	0.840	0.943	3.96	16.4	1.47	59.7	0.300
Kin08	1.50	4.80	0.840	0.943	3.96	16.4	1.47	36.6	0.300
Kin09	1.50	4.80	0.840	0.943	3.96	16.4	1.45	63.6	0.400
Kin10	1.50	4.80	0.840	0.943	3.96	16.4	1.45	32.7	0.400
Kin11	1.50	1.25	0.840	0.101	0.41	120.	1.45	29.1	0.400
Kin12	1.50	4.80	0.840	0.943	3.96	16.4	1.44	67.6	0.500
Kin13	1.50	4.80	0.840	0.943	3.96	16.4	1.44	28.7	0.500
Kin14	1.50	1.25	0.840	0.101	0.41	120.	1.44	33.1	0.500

Table 2
High Missing Momentum Kinematics

Kinematics	$\mathbf{q}$ [GeV/c]	E_o [GeV]	ω [GeV]	ϵ	E_e [GeV]	θ_e [deg.]	P_p [GeV]	θ_p [deg.]	p_m [GeV/c]
Kin15	1.50	4.80	0.840	0.943	3.96	16.4	1.41	71.7	0.600
Kin16	1.50	4.80	0.840	0.943	3.96	16.4	1.37	78.0	0.750
Kin17	1.50	4.80	0.840	0.943	3.96	16.4	1.32	84.7	0.900
Kin18	1.50	4.80	0.840	0.943	3.96	16.4	1.26	91.8	1.050
Kin19	1.50	4.80	0.840	0.943	3.96	16.4	1.19	99.6	1.200

Table 3
Parallel Kinematics

Kinematics	$\mathbf{q}$ [GeV/c]	E_o [GeV]	ω [GeV]	ϵ	E_e [GeV]	θ_e [deg.]	P_p [GeV]	θ_p [deg.]	p_m [GeV/c]
Kin20	1.00	4.05	0.453	0.966	3.59	13.4	1.00	56.6	0.000
Kin21	1.00	0.845	0.453	0.210	0.392	102	1.00	22.6	0.000
Kin22	2.00	4.80	1.29	0.890	3.51	21.5	1.94	39.9	0.000
Kin23	2.00	1.95	1.29	0.260	0.659	84.7	1.94	19.2	0.000
Kin24	3.00	4.80	2.23	0.716	2.58	33.3	3.00	28.1	0.000
Kin25	3.00	2.90	2.23	0.174	0.675	92.0	3.00	13.0	0.000

Table 4
High Missing Momentum Parallel Kinematics ($x_B = 1.86$)

Kinematics	$\mathbf{q}$ [GeV/c]	E_o [GeV]	ω [GeV]	ϵ	E_e [GeV]	θ_e [deg.]	P_p [GeV]	θ_p [deg.]	p_m [GeV/c]
Kin26	1.50	4.80	0.556	0.946	4.24	17.8	1.10	59.7	0.400
Kin27	1.50	1.25	0.556	0.253	0.693	96.9	1.10	25.4	0.400

Table 5
Singles rates for the perpendicular kinematics.

Kinematics	(e,e′p) KHz	(e,π^-) KHz	(e,p) KHz	(e,π^+) KHz
Kin01	12	18	96	25
Kin02	<1	<1	<1	<1
Kin03	12	18	<1	<1
Kin04	12	18	13	26
Kin05	12	18	<1	<1
Kin06	12	18	135	26
Kin07	12	18	<1	<1
Kin08	12	18	150	27
Kin09	12	18	<1	<1
Kin10	12	18	160	27
Kin11	<1	<1	5.	<1
Kin12	12	18	<1	<1
Kin13	12	18	200	28
Kin14	<1	<1	3.	<1

Table 6
Singles rates for the high missing momentum.

Kinematics	(e,e′p) KHz	(e,π^-) KHz	(e,p) KHz	(e,π^+) KHz
Kin15	12	18	<1	<1
Kin16	12	18	<1	<1
Kin17	12	18	<1	<1
Kin18	12	18	<1	<1
Kin19	12	18	<1	<1

Table 7
Singles rates for the parallel kinematics.

Kinematics	(e,e′p) KHz	(e,π^-) KHz	(e,p) KHz	(e,π^+) KHz
Kin20	165	19	98	21
Kin21	<1	<1	206	<1
Kin22	1.4	23	100	27
Kin23	<1	6	48	<1
Kin24	<1	22	93	<1
Kin25	<1	8	53	<1

Table 8
Singles rates for the high missing momentum.

Kinematics	(e,e′p)	(e,π^-)	(e,p)	(e,π^+)
Kin26	< 1	<1	3	18
Kin27	<1	<1	98	8

Table 9
Perpendicular kinematics.

Kinematics	p_m [GeV/c]	$\sigma 5$ [b/GeV/sr]	Coinc. [1/hr]	Time [hr]	$\delta\sigma 5$	δR_{TL}	δR_T	δR_{L+TT}
Kin01	0.000	0.370E-05	0.377E+07	1.0	<1%	N/A	2.6%	11.1%
Kin02	0.000	0.759E-07	0.252E+05	1.0	<1%			
Kin03	0.100	0.184E-05	0.187E+07	1.0	<1%	9.7%		
Kin04	0.100	0.131E-05	0.134E+07	1.0	<1%			
Kin05	0.200	0.209E-06	0.211E+06	1.0	<1%	5.2%		
Kin06	0.200	0.108E-06	0.109E+06	1.0	<1%			
Kin07	0.300	0.234E-07	0.234E+05	1.0	<1%	3.9%		
Kin08	0.300	0.894E-08	0.896E+04	1.0	<1%			
Kin09	0.400	0.259E-08	0.256E+04	16.	<1%	4.3%	6.5%	18.0%
Kin10	0.400	0.758E-09	0.749E+03	8.0	1%			
Kin11	0.400	0.376E-10	0.125E+02	46.	4%			
Kin12	0.500	0.521E-09	0.507E+03	21.	<1%	7.5%	12.1%	30.0%
Kin13	0.500	0.121E-09	0.117E+03	15.	2%			
Kin14	0.500	0.719E-11	0.239E+01	64.	8%			

Table 10
High Missing Momentum.

Kinematics	p_m [GeV/c]	$\sigma 5$ [b/GeV/sr]	Coinc. [1/hr]	Time [hr]	$\delta\sigma 5$
Kin15	600	0.127E-09	0.121E+03	4.0	4%
Kin16	750	0.167E-10	0.153E+02	10.0	8%
Kin17	800	0.164E-11	0.143E+01	16.0	20%
Kin18	1050	0.200E-12	0.163E+00	30.0	44%
Kin19	1200	0.186E-13	0.140E-01	40.0	—

Table 11
Parallel kinematics.

Kinematics	p_m [GeV/c]	$\sigma 5$ [b/GeV/sr]	Coinc. [1/hr]	Time [hr]	$\delta\sigma 5$	δR_T	δR_L	$\delta R_L/R_T$
Kin20	0.000	0.275E-04	0.163E+08	1.0	<1%	3.0%	9.2%	11.7%
Kin21	0.000	0.448E-06	0.142E+06	1.0	<1%			
Kin22	0.000	0.637E-06	0.933E+06	1.0	<1%	3.2%	27.5%	30.4%
Kin23	0.000	0.392E-07	0.209E+05	1.0	<1%			
Kin24	0.000	0.418E-07	0.871E+05	1.5	<1%	3.1%	55.0%	57.7%
Kin25	0.000	0.589E-08	0.322E+04	3.5	<1%			

Table 12
High Missing Momentum Parallel kinematics ($x_B = 1.86$)

Kinematics	p_m [GeV/c]	$\sigma 5$ [b/GeV/sr]	Coinc. [1/hr]	Time [hr]	$\delta\sigma 5$	δR_T	δR_L	$\delta R_L/R_T$
Kin26	0.400	0.706E-09	0.957E+02	14.	2.7%	7.2%	45.8%	56.0%
Kin27	0.400	0.273E-10	0.153E+02	31.	4.6%			

Table 13
Additional Kinematics To Be Done During E07-006 ($x_B = 1.2$)

Kinematics	**q** [GeV/c]	E_o [GeV]	ω [GeV]	E_e [GeV]	θ_e [deg.]	P_p [GeV]	θ_p [deg.]	p_m [GeV/c]	$\sigma 5$	Time [hr]
Kin28	1.6	4.80	0.850	3.95	18.7	1.6	50.1	0.100	<1%	1.0
Kin29	1.6	4.60	0.850	3.95	18.7	1.5	45.4	0.200	<1%	2.0
Kin30	1.6	4.80	0.850	3.95	18.7	1.4	41.0	0.300	<1%	8.0

8.4 Additional Cross Section Measurement

In addition to the kinematics that match the work done on ^{3}He(e,e′p), we are asking for 0.5 PAC days to do three additional (e,e′p) cross section measurements as a short extension of the recently approved (e,e′pN) E07-006 experiment. As the E07-006 experiment is focused on triple coincidence events, they only requested to measure the (e,e′p) reaction in the p_m range from 400-900 MeV/c. Our measurements will extend this to coverage over the entire p_m range and are summarised in Table 13.

All the equipment that is needed to do these extra cross section measurements will be installed for the E07-006 experiment, thus very little extra time is needed. In these high Q^2 and x>1 kinematics, as one goes to p_m greater than the Fermi momentum, tensor correlations are expected to dominate the reaction. The extra measurements will map this transition and will further test the theoretical models.

We ask for an additional 1 hr of beam time to do carbon pointing measurements. Note that we are not using either BigBite or Neutron array needed for E07-006; though those detectors could be tested while these measurements are being made with the HRS.

8.5 Systematic and Statistical Uncertainties

With careful luminosity monitoring and elastic cross section measurements at appropriate energies we should be able to achieve a systematic uncertainty of 2% as exhibited in the E89-044 experiment on ^{3}He. We have therefore assumed a systematic uncertainty of 2% for all our cross section measuremets. In Tables 9, 10 and 11 the uncertainty in the five-fold differential cross sections, denoted as $\sigma 5$, includes only the statistical uncertainty, while the uncertainty for the response functions includes both statistical and systematic uncertainties.

In Fig. 18 and Fig. 17 the coincidence rate and the accidental rate is plotted for the parallel and perpendicular kinematics. Even for our most extreme kinematics the signal to accidental ratio is greater than one. Further, it is possible to reduce the accidentals by a factor of 5 by requiring a consistent vertex from both spectrometers and another factor

of 10 from a missing mass cut.

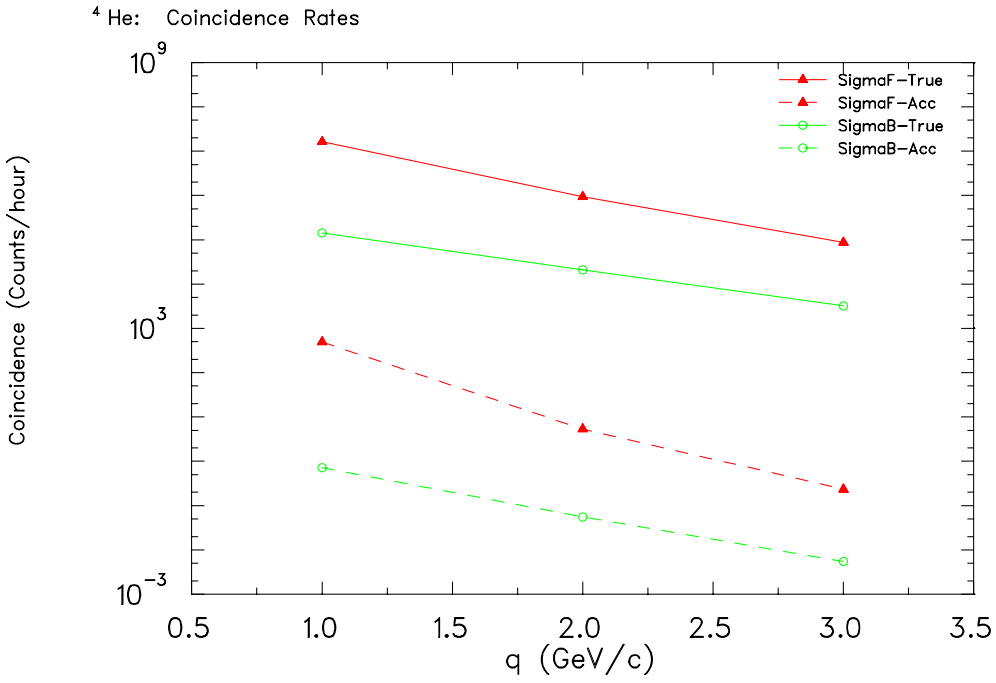

Fig. 17. The coincidence and accidentanl rates are shown for the parallel kinematics.

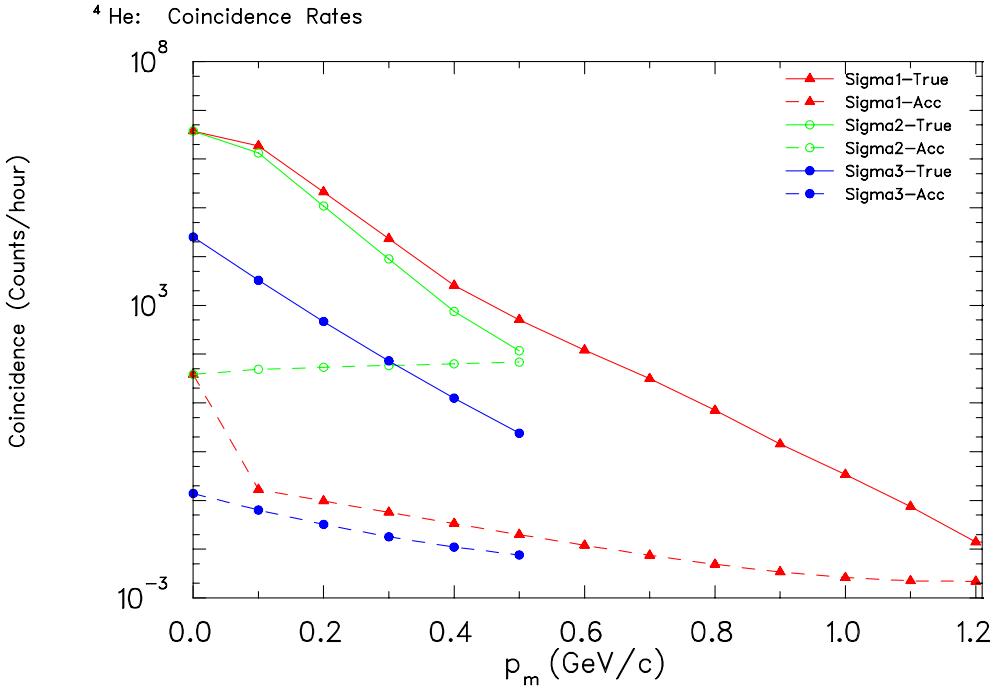

Fig. 18. The coincidence and accidental rates are shown for the perpendicular kinematics.

9 Expected Results

On the following pages the expected results from the proposed measurements are shown along with the calculations of J.M. Udias and J.M. Laget. The shaded region on the figures indicates the range in p_m for which R_{TL}, R_T, and R_{L+TT} will be extracted. Figures 19, 20, and 21 show the expected cross section results, figure 22 shows the expected A_{TL} results, and figures 23, and 24 show the expected response function separation results. It is worth pointing out that while two completely different approaches are being used, these calculations agree rather well for missing momenta less then 300 MeV/c for both cross sections and in the response functions.

In the figures, the Udias-RDWIA curves corresponds to the fully relativistic calculation described in section 7.1. The RPWIA curves are also a fully relativistic calculation, but with the outgoing proton treated as a free Dirac particle, i.e. no distortions and no negative energy components. The bound state, however, is still treated as a bound Dirac particle, so it still contains negative energy components. For the Udias-EMAnoSV curves the negative energy components of the bound proton and outgoing proton are projected out and only the positive energy components are used, and outgoing proton is treated as a plane wave Dirac spinor. Also the effective momentum approximation (EMA) with no spinor distortion (no SV) is used, which means the bound proton and continuum proton have the same upper/lower spinor component ratios as for free particles and that asymptotic values of the momenta are used. The Laget-Full curves includes all two- and three-body mechanisms described in section 7.2 while the Laget-PWIA curves includes only the one-nucleon exchange amplitude.

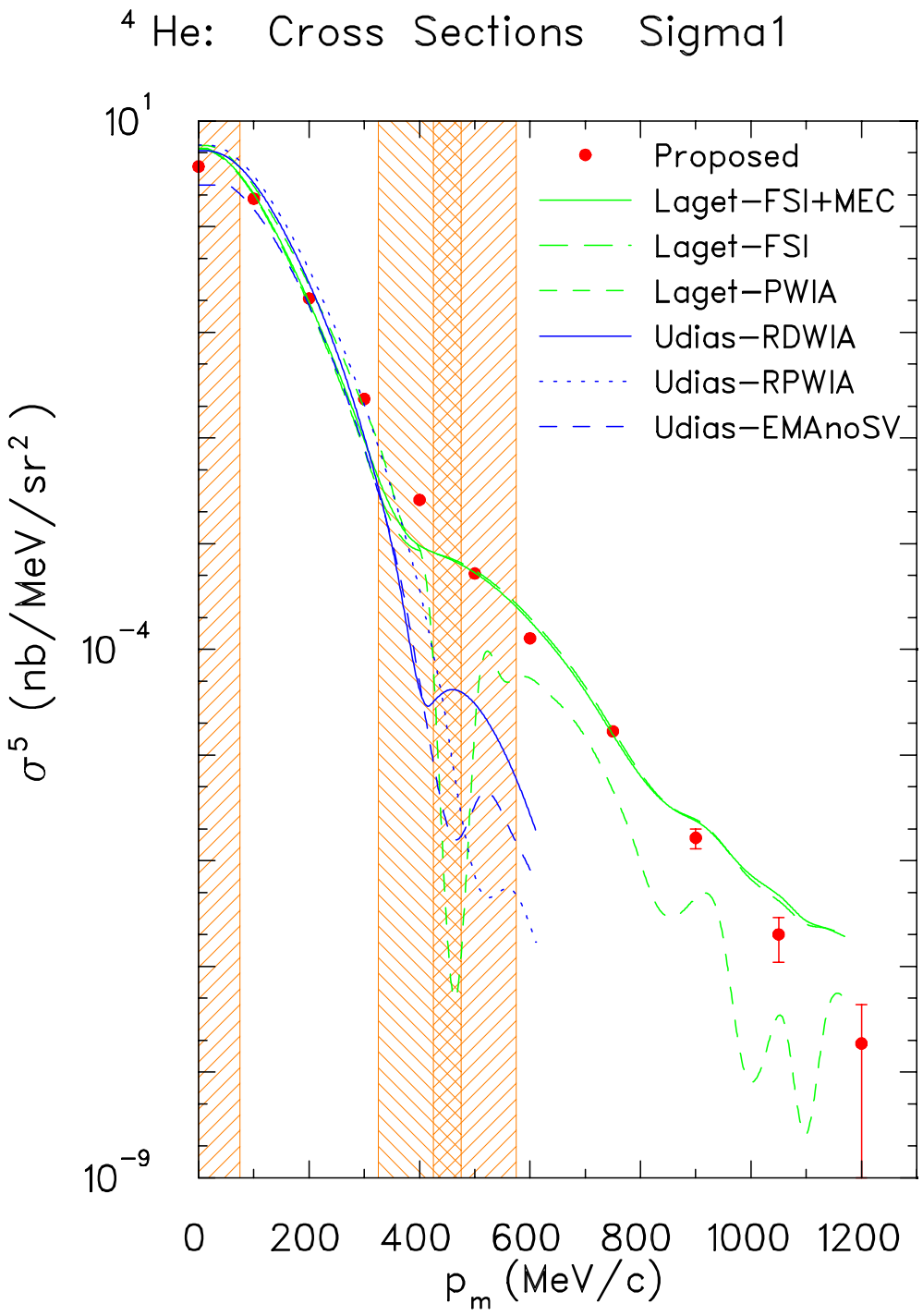

Fig. 19. The expected data are shown for the perpendicular kinematics, $\mathbf{q}$ = 1.5 GeV/c and ω = 0.84 GeV, with ϵ = 0.943 and ϕ = 180°. In this kinematics, denoted as $\Sigma 1$, the data up to 0.50 GeV/c will be used to determine the R_{TL}, R_T, and R_{L+TT} response function separations and to extract the A_{TL} asymmetry, while the higher p_m data will be used solely as a cross section measurement.

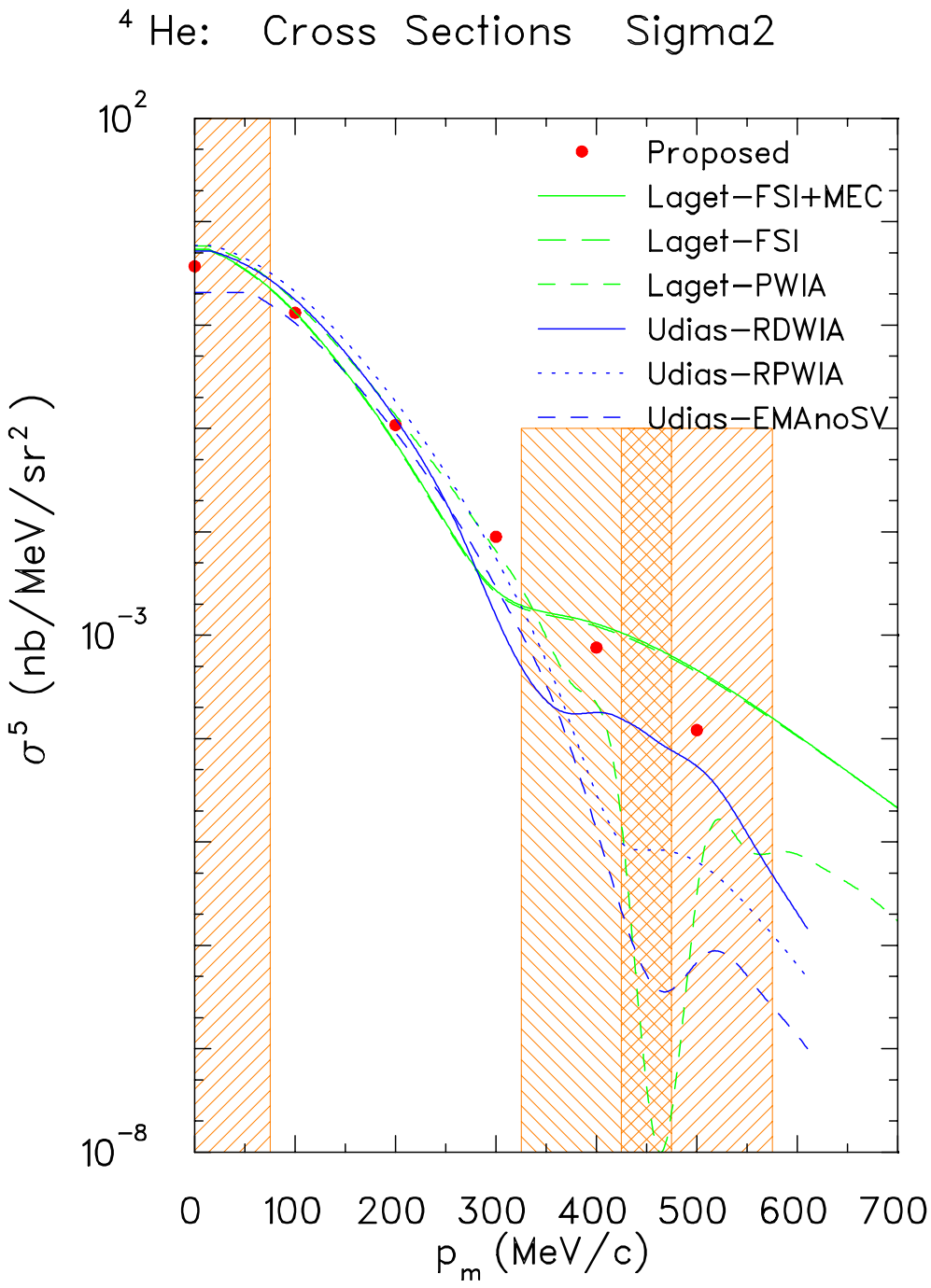

Fig. 20. The expected data are shown for the perpendicular kinematics, $\mathbf{q} = 1.5$ GeV/c and $\omega = 0.84$ GeV, with $\epsilon = 0.943$ and $\phi = 0°$. In this kinematics, denoted as $\Sigma 2$, the data will be used for the R_{TL}, R_T, and R_{L+TT} response function separations and to extract the A_{TL} asymmetry.

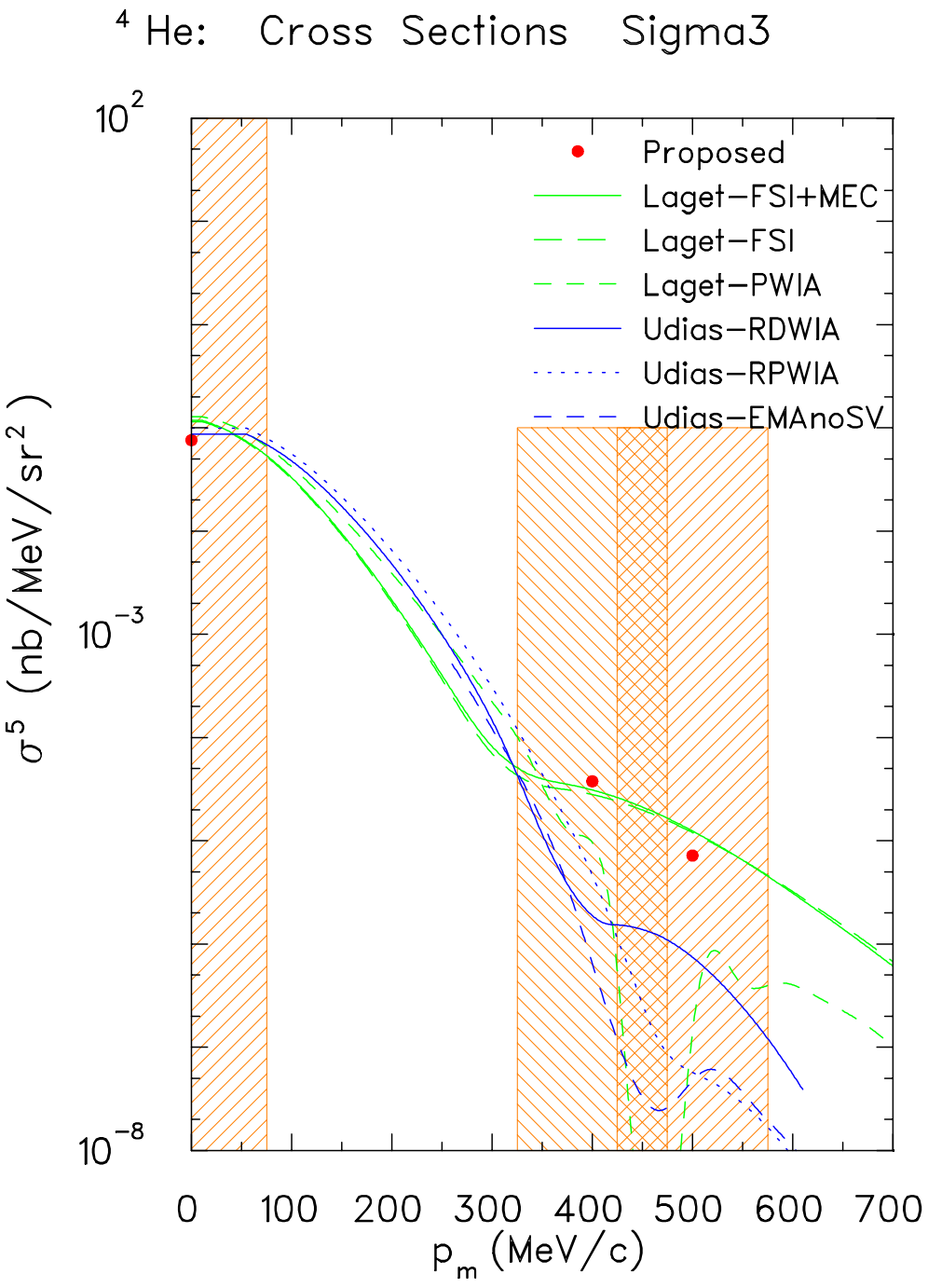

Fig. 21. The expected data are shown for the perpendicular kinematics, $\mathbf{q}$ = 1.5 GeV/c and ω = 0.84 GeV, with ϵ = 0.108 and ϕ = 180°. These data points will be used in order to make the R_T and R_{L+TT} separations.

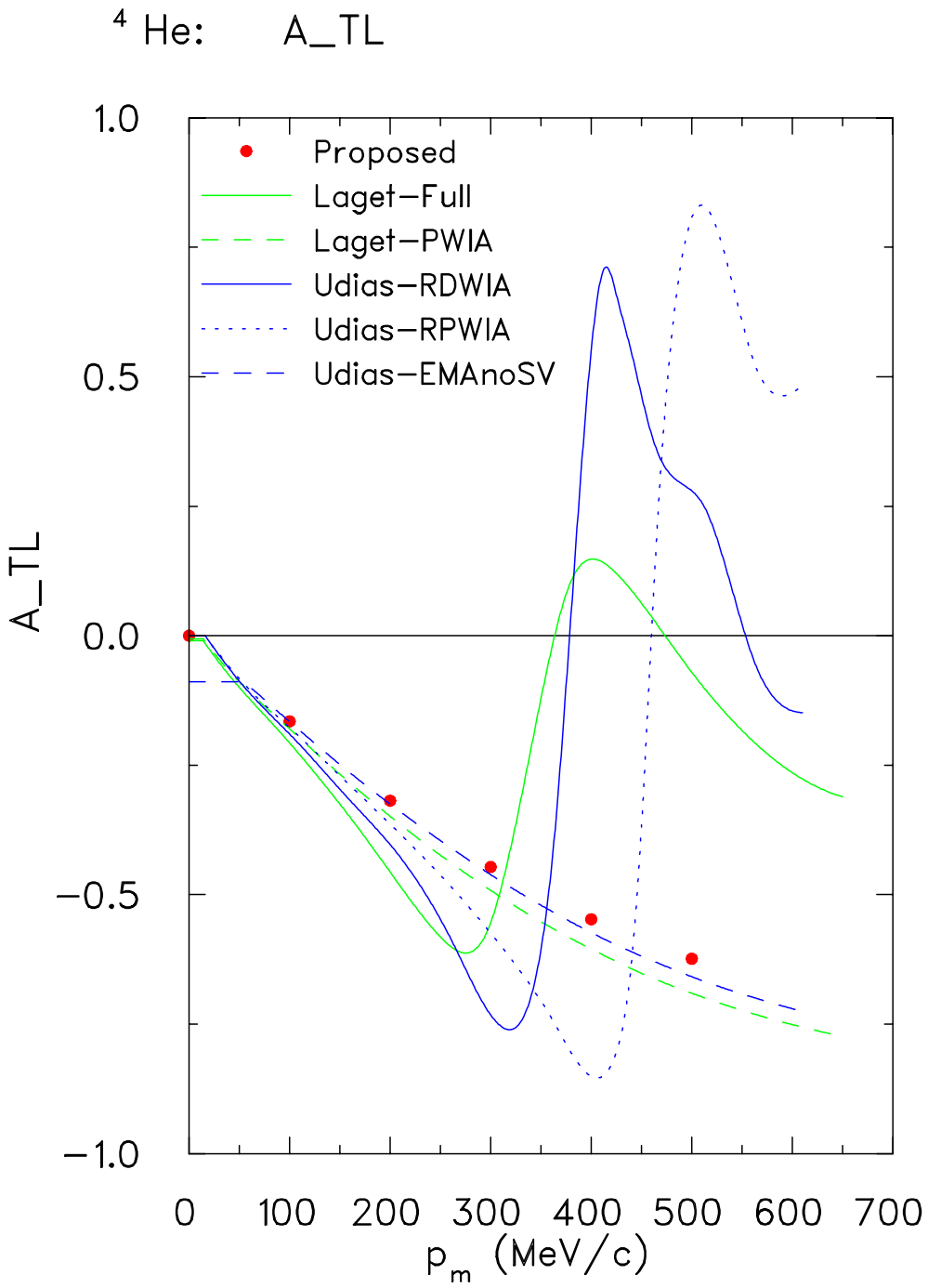

Fig. 22. Shown is the expected A_{TL} asymmetry extracted from the $\Sigma 1$ (see figure 19) and $\Sigma 2$ (see figure 20) cross section measurements. Both the full calculations of J.M. Udias and J.-M. Laget predict this asymmetry to be very sensitive to the "dip" in the PWIA cross section. It is worth noting, that in PWIA the calculations show A_{TL} to be completely insensitive to the dip.

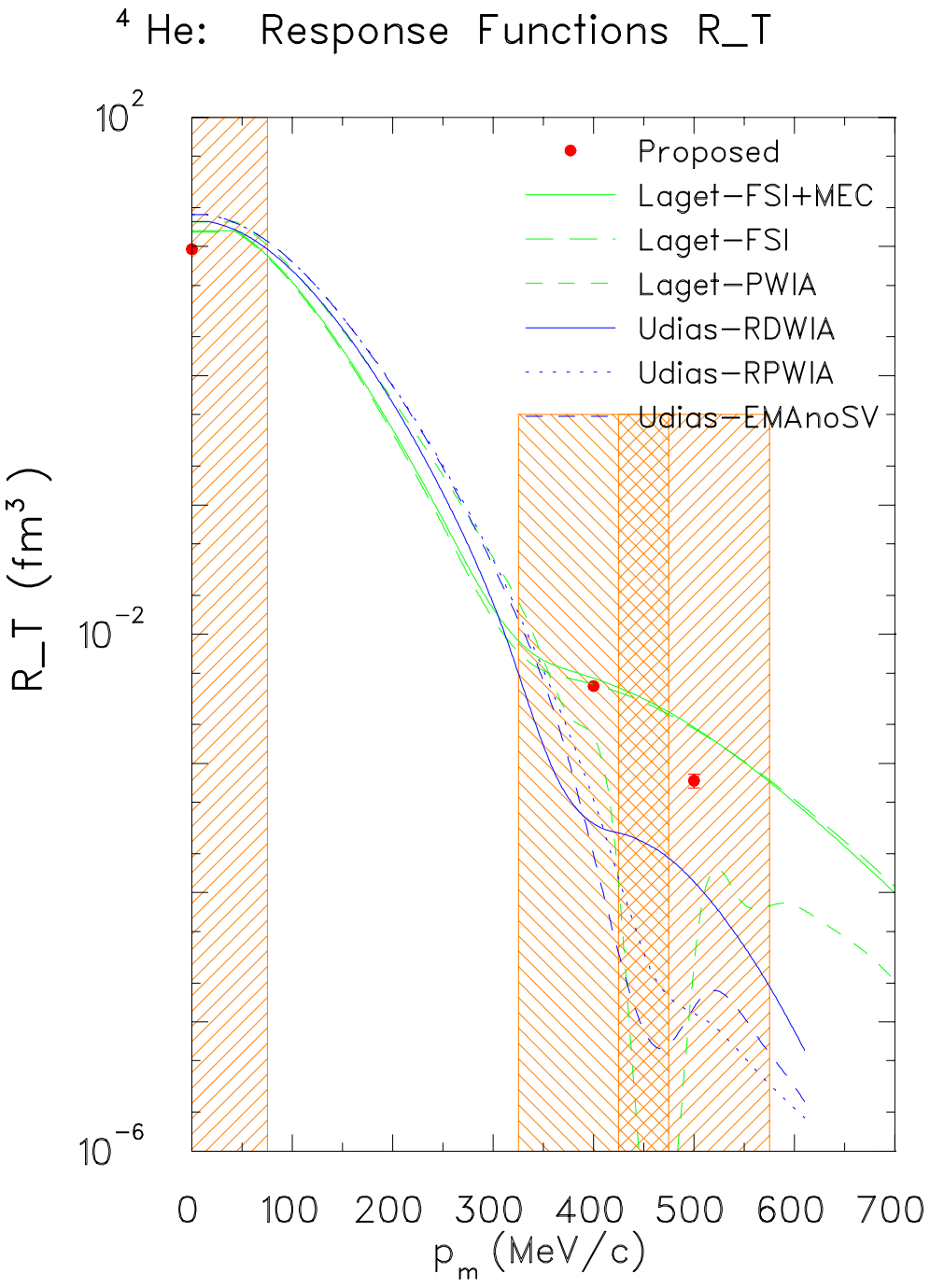

Fig. 23. Shown is the expected result of R_T response function separations determined using the cross sections from $\Sigma 1$ (see figure 19) and from $\Sigma 3$ (see figure 21) kinematics.

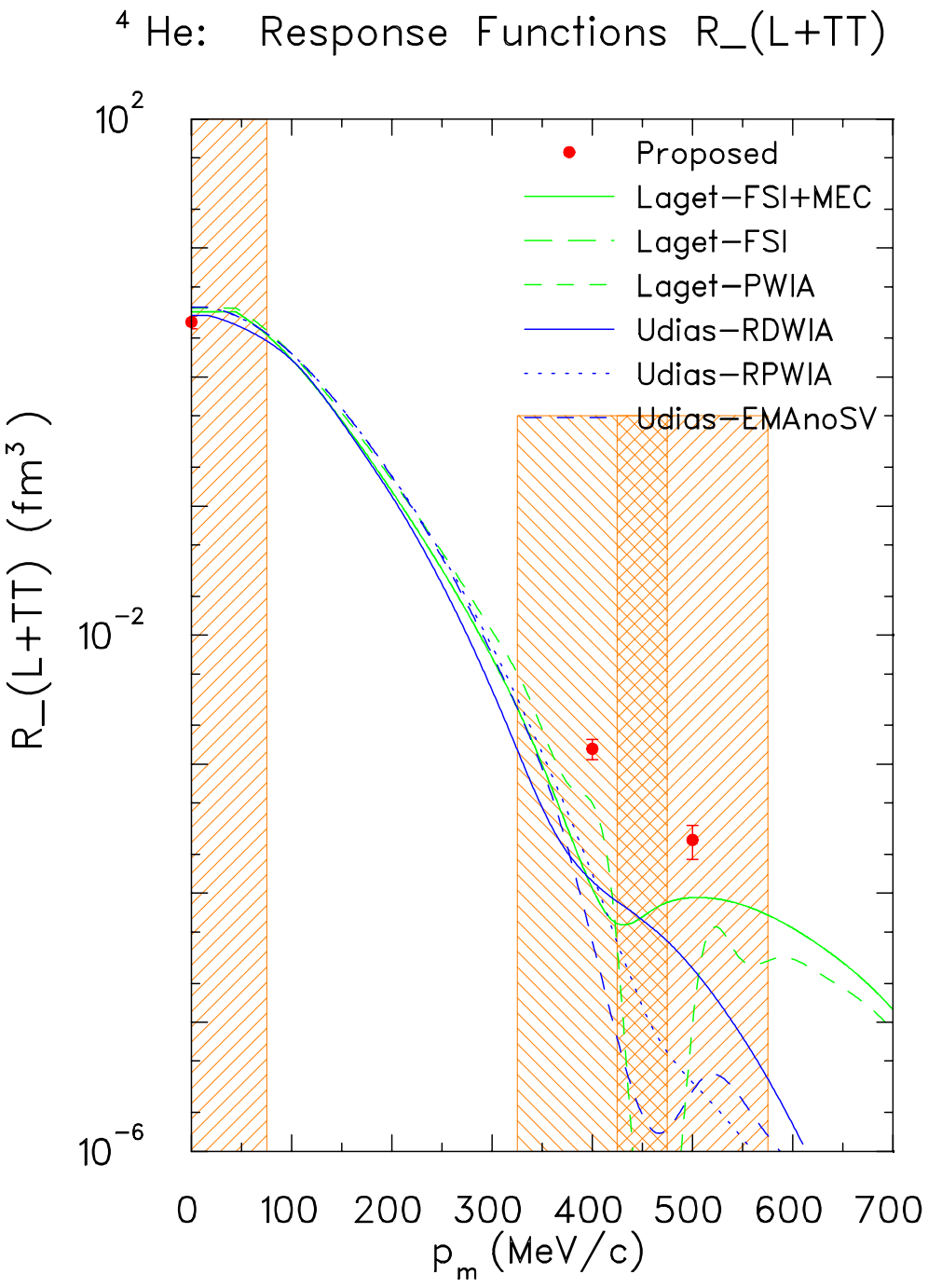

Fig. 24. Shown is the expected result of R_{L+TT} response function separations determined using the cross sections from $\Sigma 1$ (see figure 19) and from $\Sigma 3$ (see figure 21) kinematics.

10 Beamtime Request

To perform this experiment and make the necessary systematic measurements, we request 20.5 days of beamtime, as shown in Table 10. The time estimates in Tables 9, 10, and 11 have been adjusted up by 30% to account for radiative losses. The table shows all necessary time, including the time to move the spectrometers. The different energies needed by this experiment only require a different pass beam to be sent to Hall A, except for the 1.25 GeV beam.

Cross Section Measurements	435 hrs
Spectrometer Field and Position Changes	16 hrs
ARC and EP Energy Measurements	12 hrs
ARC and EP Energy Measurements	17 hrs
Elastic Scattering Measurements	12 hrs
Total	492 hrs (20.5 days)

Table 14
Time requested for the ^{4}He(e,e′p)^{3}H response function seperation experiment.

We will preform these ARC and EP energy measurments for each beam energy. Each measurment take approximately one hour, therefore we request 12 hrs to perform these measurements. For each position of the spectrometers, we will take carbon pointing data. For these measurements we measure ^{12}C(e,e′) and ^{12}C(e,p) from a multifoil carbon target. This allows us to calibrate the pointing of the spectrometers for each kinematics. This method has shown itself to agree with survey data while taking less time. These measurments take approximately 1/2 hour each and we therefore request 16 hrs to perform them.

The final item is performing elastic scattering measurments. By making measurements of the well known elastic scattering, we are able to check our knowledge of the target thickness. When preforming an elastic ^{4}He(e,e′) measurement, the hadron spectrometer is placed at an angle for an upcoming ^{4}He(e,e′p) kinematics. By continously monitoring the singles rates and only moving one spectrometer at a time, we have continuous monitoring of the target thickness which links back to the elastic measurment. Only for the highest beam energy is this technique not viable, since the Hall A electron spectrometers can only achieve momenta of approximately 4.2 GeV/c. For this particular case, we measure elastic scattering from the target with a lower beam energy immediately before and after the 4.8 GeV/c run period. By monitoring the temperature and pressure of the target during the energy change, we can account for target density changes, although during the E89-044 experiment no changes were observed in temperature and pressure for long periods of time and the elastic scattering measurements taken before and after the 4.8 GeV/c run period both produced the same result. For these measurments we request 16 hours.

References

[1] F. Benmokhtar, Phys. Rev. Lett **94** (2005) 082305.

[2] M. M. Rvachev, Phys. Rev. Lett **94** (2005) 192302.

[3] Marat Rvachev, Ph.D. thesis, Massachusetts Institute of Technology (2003).

[4] Emilie Penel-Nottaris, Universite′ Joseph Fourier., (2004).

[5] Fatiha Benmokhtar, Ph.D. thesis, Rutgers University (2004).

[6] J.J. van Leeuwe, Ph.D. thesis, Universiteit Utrect (1996).

[7] J.J. van Leeuwe *et al.*, Phys. Rev. Lett. **80** (1998) 2583.

[8] J. Gao *et al.*, Phys. Rev. Lett. **84** (2000) 3265.

[9] J. Templon *et al.*, Systematic Probe of Short-Range Correlations via the Reaction ^{4}He(e,e′p)^{3}H, TJNAF Hall A Proposal E97-111.

[10] J-E. Ducret *et al.*, Nucl. Phys. **A556** (1993) 373.

[11] Z.-E. Mezianni *et al.*, Nucl. Phys. **A553** (1993) 701c.

[12] J-E. Ducret *et al.*, Nucl. Phys. **A553** (1993) 697c.

[13] K. S. Egiyan *et al.*, Phys. Rev. C **68** (2003) 014313.

[14] J.W. van Orden, N. Devine and F. Gross, Phys. Rev. Lett. **75** (1995) 4369.

[15] E. Hummel and J.A. Tjon, Phys. Rev. C **49** (1994) 21.

[16] J. Golak *et al.*, Phys. Rev. **C51** (1995) 1638.

[17] R. Schiavilla, V. Pandaripande and R. Wiringa, Nucl. Phys. **A449** (1986) 219.

[18] R. Schiavilla, Phys. Rev. Lett. **65** (1990) 835.

[19] J.M. Udias *et al.*, nucl-th/0101038v3.

[20] V.D. Efros, W. Leidemann and G. Orlandini, Phys. Rev. C **58** (1998) 552.

[21] Z. Zhou *et al.*, nucl-ex/0105006.

[22] J.M. Laget, Nucl. Phys. **A579** (1994) 333.

[23] S.I. Nagorny *et al.*, Sov. J. Nucl. Phys. **49** (1989) 465.

[24] S.I. Nagorny *et al.*, Sov. J. Nucl. Phys. **53** (1991) 228.

[25] M.B. Epstein *et al.*, Phys. Rev. Lett. **70** (1993) 2868.

[26] J.M. Laget, Nucl. Phys. **A497** (1989) 391c.

[27] R.E.J. Florizone, Ph.D. thesis, Massachusetts Institute of Technology (1999).

[28] A.A. Kozlov, Ph.D. thesis, University of Melbourne (2000).

[29] A.A Kozlov *et al.*, Nucl. Phys. **A684** (2001) 460.

[30] T. de Forest, Nucl. Phys. **A392** (1983) 232.

[31] J.J. van Leeuwe *et al.*, Nucl. Phys. **A631** (1998) 593c.

[32] N. Liyanage *et al.*, Phys. Rev. Lett. (2001) 5670.

[33] J Ryckebusch *et al.*, Nucl. Phys. **A624** (1997) 581.

[34] J.M. LeGoff *et al.*, Phys. Rev. **C50** (1994) 2278.

[35] M.B. Epstein, A. Saha, R. Lourie and J. Mougey, Selected Studies of the ^{3}He and ^{4}He Nuclei through Electrodisintegration at High Momentum Transfer, TJNAF Hall A Proposal E89-044.

[36] S. Dieterich, Phys. Lett. **B500** (2001) 47.

[37] S. Strauch, Phys. Rev. Lett (2003) 052301.

[38] S. Strauch R. Ent, R. Ransome and P. Ulmer spokespersons, Probing the limites of the standard model of nuclear physics with the ^{4}he($\vec{e}$,e'$\vec{p}$)^{3}h reaction, TJNAF Hall A Proposal E03-104.

[39] B. Hu, Phys. Rev. C **73** (2006) 064004.

[40] P. Lava, Phys. Rev. C (2005) 014605.

[41] S. Strauch, Private communication.

[42] C. Ciofi degli Atti and L. P. Kaptari, Phys. Rev. Lett **95** (2005) 052502.

[43] C. Ciofi degli Atti and L. P. Kaptari, Private communication.

[44] R. Schiavilla, Phys. Rev. C **72** (2005) 064003.

[45] J. M. Udias *et al.*.

[46] J. M. Udias, J. A. Caballero, E. Moya de Guerra, J. E. Amaro and T. W. Donnelly, Phys. Rev. Lett. **83** (1999) 5451.

[47] J. M. Udias, (2004), $XXIII^{rd}$ International Workshop on Nuclear Theory. Rila, Bulgaria.

[48] J. M. Laget, Few Body Systems Supplement **15** (2003) 171.

[49] B. Hersman, Update on CEBAF Proposals PR-89-015, -017, -027, -031, -32, and -036, TJNAF Hall B Proposal E91-009.

[50] L. Weinstein, W. Bertozzi and W. Boeglin, Coincidence Reaction Studies with the LAS, TJNAF Hall B Proposal E89-027.

[51] J.M. Udias, Private communication.

[52] J.J. Kelly, Phys. Rev C **60** (1999) 044609.

[53] J.M. Udias *et al.*, Phys. Rev. C **51** (1995) 3246.

[54] S. Janssen and J. Ryckebusch, Prog. Part. Nucl. Phys. **50** (2003) 533.

[55] S. Jeschonnek and R. Schiavilla, Private communication.

[56] R.B. Wiringa, V.G.J. Stoks and R. Schiavilla, Phys. Rev. C **51** (1995) 38.

[57] S. Jeschonnek and T.W. Donnelly, Phys. Rev. C **57** (1998) 2438.

[58] S. Jeschonnek and T.W. Donnelly, Phys. Rev. C. **59** (1999) 2676.

[59] R.E.J. Florizone *et al.*, Phys. Rev. Lett. **83** (1999) 2308.

[60] J. F. J. van den Brand *et al.*, Nucl. Phys. **A534** (1991) 637.

[61] J.W. Lightbody and J.S. O'Connel, Computers in Physics, May/June (1988) 57.

[62] A. Saha, Private communication.